Placental Iron Utilisation in Fetal Growth Restriction: Alterations in Mitochondrial Heme Synthesis and Iron-Sulfur Cluster Assembly Pathways

Veronica B Botha[1,2], Heather C Murray[1,3], Siddharth Acharya[1,2], Kirsty G Pringle[1,4], Roger Smith*[2,5], Joshua J Fisher*[2,5].

[1]School of Biomedical Sciences and Pharmacy, University of Newcastle, Callaghan, New South Wales, Australia

[2]School of Medicine and Public Health, University of Newcastle, Callaghan, New South Wales, Australia

[3] Precision Medicine Program, Hunter Medical Research Institute, New Lambton Heights, New South Wales, Australia

[4]Women's Health Research Program, Hunter Medical Research Institute, New Lambton Heights, New South Wales, Australia

[5]Mothers and Babies Research Program, Hunter Medical Research Institute, New Lambton Heights, New South Wales, Australia

***denotes equal contribution as senior author**

Corresponding Author:

Dr Joshua Fisher

Postdoctoral Research Fellow

Mothers and Babies Research Centre

Hunter Medical Research Institute

Faculty of Health and Medicine | School of Medicine and Public Health

Joshua.fisher@newcastle.edu.au, https://orcid.org/0000-0002-0505-0598

Key Points

- Iron plays a critical role in placental function, while iron-dependent pathway components are well-characterised, their integrated response and adaptive reprogramming in fetal growth restriction (FGR) remain poorly understood.
- In FGR, maternal iron status was unchanged, however, placental iron uptake proteins were increased and ferroportin reduced, suggesting that the placenta retains iron.
- FGR placentae showed altered de novo mitochondrial iron-sulfur cluster (Fe-S) formation and a bottleneck in late-stage Fe-S cluster assembly.
- This shift in Fe-S synthesis prioritises mitochondrial and cytosolic heme synthesis pathways, consistent with increased heme utilisation and breakdown.

- Globin subunits were lower in protein abundance and impaired placental erythrocyte structure in FGR.
- Dysregulation of erythrocyte membrane proteins in FGR placentae suggests altered erythrocyte structure, potentially representing an adaptive response to inadequate vascularisation, attempting to optimise oxygen delivery to the fetus.

Abstract

Fetal growth restriction (FGR) affects ~10% of pregnancies worldwide and is often associated with placental insufficiency. Iron is essential for maternal haematopoietic adaptations and placental processes such as mitochondrial iron–sulfur (Fe-S) cluster assembly, heme synthesis, and erythropoiesis. This study aimed to characterise iron transport and downstream utilisation in FGR. Placental tissues from term uncomplicated (n=19) and FGR (n=18) pregnancies were analysed. Maternal iron status was retrospectively assessed from clinical records. Placental mRNA and protein expression of iron-dependent pathways were analysed via RT-qPCR, LC-MS, and western blotting. Placental iron content was assessed histologically, and heme levels were measured by activity assay. FGR pregnancies showed significantly elevated maternal serum ferritin and lower red cell distribution width, although remained within normal clinical values. Placental iron uptake transporters TFRC and DMT1 were significantly upregulated, while the iron exporter to the fetus, ferroportin, was reduced, indicating increased iron retention in the FGR placenta. Despite altered transporter expression, Fe^{3+} iron levels were unchanged, suggesting iron utilisation over storage. Subsequent investigations identified reduced mitochondrial Fe-S synthesis components (FDXR, FDX2, NDUFAB1, HSPA9), and a prioritisation of mitochondrial and cytosolic heme synthesis enzymes in FGR. Protein levels of haemoglobin subunits (HBG1, HBG2, HBB, HBA1) and erythrocyte membrane markers (EPB41, EPB42, SPTA1, SPTB, ANK1) were decreased. These findings reveal a compensatory response in FGR placentae, with increased iron uptake and utilisation favouring heme synthesis over Fe-S cluster formation, possibly to support oxygen handling under poor placental vascularisation and reduced fetal oxygenation, with potential consequences for mitochondrial energy metabolism.

Introduction

Fetal growth restriction (FGR) occurs in 10% of pregnancies globally and is associated with increased perinatal and neonatal morbidity and mortality (Miller *et al.*, 2008). FGR is defined by the inability of the fetus to achieve its genetically predetermined growth potential relative to its gestational age (Gordijn *et al.*, 2016). Although maternal and fetal complications are recognised causes of FGR, 60-70% of FGR cases are associated with placental insufficiency, where the placenta fails to adequately deliver nutrients and oxygen, arising from inadequate uterine spiral artery remodelling (Brooker *et al.*, 2025; Higashijima *et al.*, 2013; Tang *et al.*, 2017). In FGR placentae, the cellular landscape is altered, with impaired cytotrophoblast maturation and decreases in trophoblast volume. This results in a reduction in the number of placental villi and a decreased placental diameter (Sun *et al.*, 2020). Consequently, the surface area available for oxygen and nutrient exchange is diminished, limiting substrate transfer to the fetus (Zygmunt *et al.*, 2003). In response, the fetus adapts by redistributing blood flow, prioritising essential fetal organs, such as the brain and heart, resulting in asymmetrical growth and slowing the fetal growth rate (Miller *et al.*, 2008; Roberts *et al.*, 2020; Wu *et al.*, 2023).

The placenta is a highly vascularised, potent haematopoietic organ. The placenta performs primitive haematopoiesis during embryogenesis, establishing a large reservoir of haematopoietic stem cells (HSCs) that not only support erythrocyte activity during early gestation, but also provide progenitor cells for the fetal liver and bone marrow when haematopoiesis transitions away from the placenta (Gekas *et al.*, 2010; Palis & Segel, 1998). Hematopoietic function is critically reliant on iron availability, as iron is essential for erythropoiesis and mitochondrial functions that facilitate the biosynthesis of iron-sulfur clusters (Fe-S) and subsequent heme synthesis in erythroid cells (Chiabrando *et al.*, 2014; Hentze *et al.*, 2004; Mastrogiannaki *et al.*, 2009).

Iron is an essential micronutrient for both fetoplacental development and mitochondrial bioenergetics (Dev & Babitt, 2017; Guo *et al.*, 2019). During pregnancy, the requirement for iron alters as gestation advances. In early pregnancy, placental development occurs in a physiologically hypoxic environment, with relatively low iron demands (Guo *et al.*, 2016). This low-oxygen environment stabilises hypoxia inducible factors (HIFs), which transcriptionally activate genes involved in oxygen and iron regulation, such as erythropoietin (EPO), hepcidin and erythroferrone (Semenza, 2014). In the first trimester, rising EPO levels support both maternal erythropoiesis and transient placental hematopoietic activity (Cindrova-Davies & Sferruzzi-Perri, 2022; Delaney *et al.*, 2021; Fairchild Benyo & Conrad, 1999). Consequently,

hepcidin is suppressed, enhancing maternal iron mobilisation and supporting the increase in maternal iron demands to meet increased cardiovascular, renal, and haematological adaptations, as well as fetoplacental development (Zaugg *et al.*, 2022). These adaptations require sufficient iron for enhanced haematopoiesis and haemoglobin synthesis. Subsequently, this supports optimal oxygen transfer, thereby sustaining fetal development, while also establishing fetal iron reserves in the later stages of gestation (Cao & Fleming, 2016; Roberts et al., 2020). Maternal iron deficiency, anaemia and excess iron alike have been implicated in adverse pregnancy outcomes, including FGR (Andrews, 2000), highlighting the important role of iron in healthy pregnancies.

Iron transport during pregnancy occurs unidirectionally from the mother to the fetus, primarily via transferrin-bound iron in the maternal circulation (McArdle *et al.*, 2003). At the maternal placental interface, transferrin receptor 1 (TfR1/TFRC) binds the maternal transferrin-iron complex, inducing endocytosis (McArdle *et al.*, 2011; Roberts *et al.*, 2020). Within the endosome, the acidic pH induces a conformational change in TfR1, releasing ferric (Fe^{3+}) iron. Following the conversion of Fe^{3+} to ferrous (Fe^{2+}) iron, iron is transported into the cytosol via divalent metal transporter 1 (DMT1) (McArdle *et al.*, 2011; Roberts *et al.*, 2020; Waldvogel-Abramowski *et al.*, 2014). Once in the cytosol, iron has three potential fates, it is either: (i) stored in ferritin, (ii) shuttled to the mitochondria for iron-sulfur (Fe-S) cluster biogenesis and heme synthesis, or (iii) transported across the basolateral (fetal) membrane via ferroportin for entry into the fetal circulation following reoxidation to Fe^{3+} (McArdle *et al.*, 2011; Roberts *et al.*, 2020). Approximately 20-50% of cellular iron is directed towards the mitochondria to support two critical pathways, the biosynthesis of Fe-S clusters and heme (Qi *et al.*, 2023; Roberts *et al.*, 2020)

Fe-S clusters are diverse molecular structures that perform various biological functions within the cell. Specifically, Fe-S clusters play a role within the mitochondrial electron transport chain (ETC), via redox reactions that transfer electrons and generate a proton gradient essential for ATP synthesis (Mostajabi Sarhangi & Matyushov, 2023; Paul *et al.*, 2017). De novo Fe-S cluster synthesis begins with the formation of [2Fe-2S] clusters, which serve as essential precursors in the Fe-S cluster pathway. These de novo [2Fe-2S] clusters undergo further processing to generate more complex [3Fe-4S] and [4Fe-4S] clusters downstream. These late-stage [3Fe-4S] and [4Fe-4S] clusters are critical for the function and stability of the mitochondrial ETC, particularly in complexes I, II and III, where they facilitate efficient electron transfer during oxidative phosphorylation (Maio & Rouault, 2020; Mostajabi Sarhangi

& Matyushov, 2023; Read *et al.*, 2021). Additionally, the terminal enzyme in heme biosynthesis, ferrochelatase (FECH), requires [2Fe-2S] clusters for its activity, linking Fe-S cluster synthesis with heme production. Heme is essential for oxygen transport through its incorporation into haemoglobin and cytochromes, which facilitate electron transfer in the ETC, particularly complexes II, III, and IV (Anderson & Frazer, 2017; Kim *et al.*, 2012).

The primary utilisation of iron in fetal development is in erythropoiesis (Cerami, 2017), and heme stimulates the production of α- and β-like globin genes with distinct haemoglobin profiles expressed at specific stages of gestation (Kim *et al.*, 2012; Moksnes *et al.*, 2022) . Embryonic (ζ2ε2) and fetal (α2γ2) haemoglobin exhibit higher oxygen affinity compared to adult (α2β2) haemoglobin, demonstrated by a leftward shift in their oxygen dissociation curves. These haemoglobin variants exhibit higher oxygen affinities during early development, enabling adaptation to lower oxygen availability and efficient maternal–fetal oxygen transfer (Manning *et al.*, 2020).

Despite the well-described crucial role of iron in placental and fetal development, the specific alterations in iron-dependent pathways in FGR placentae remain uncharacterised. The complex interplay between iron transport, Fe-S cluster assembly, and heme synthesis is particularly relevant in the context of FGR, where placental insufficiency and impaired oxygen delivery are defining clinical characteristics. We have therefore examined genes and proteins involved in placental iron transport, as well as iron-related mitochondrial proteins involved in Fe-S assembly, heme synthesis, and placental erythropoiesis in FGR compared to healthy placentae. Collectively, these results provide molecular insights into how altered iron transport and iron-dependent pathways may contribute to mitochondrial dysfunction and placental insufficiency observed in FGR.

Methodology

Ethical Approval

Ethical approval for this research was obtained from the University of Newcastle Human Research Ethics Committee (H-382-0602), Hunter New England Health Human Research Ethics Committee (02/06/12/3.13), and Site-Specific Assessment (SSA/15/HNE/291), in compliance with the Declaration of Helsinki. Informed consent was obtained from all participants.

Maternal and Placental Sample Collection

Placental villous cores were collected from 19 healthy, uncomplicated and 18 FGR (percentiles: <3rd n=7, <5th n=2 and <10th n=9) pregnancies within 45 minutes of birth as previously described by Fisher *et al.* (2024) and washed in ice-cold PBS to limit maternal blood contamination. Tissues were either preserved in formalin at 4°C overnight and stored in 0.1 M PBS with 0.05% sodium azide for histological analysis, or snap-frozen and stored at -80°C for later gene and protein analysis. FGR was diagnosed with consensus criteria as published by Gordijn *et al.* (2016). All placentae collected for this study met the eligibility criteria. Healthy term pregnancies were from singleton deliveries between 37- 40 weeks of gestation. FGR cases were from singleton pregnancies delivered by caesarean section at 34-40 weeks of gestation with an estimated fetal weight <10th centile and birthweight confirmed <10th centile. Exclusion criteria applied to all samples with premature membrane rupture, hypertension, diabetes, placental abnormalities, chorioamnionitis, immune deficiencies, infectious diseases, smoking, non-steroidal anti-inflammatory drug use, illicit drug use, and metformin use were not eligible within our study. Maternal blood samples collected as part of routine care were analysed retrospectively to assess clinical iron parameters. Reference ranges were obtained using New South Wales Health Pathology (NSWHP) Hospital Laboratory Clinical Projects Laboratory Manual (Brighton, 2019) in conjunction with Pregnancy and Laboratory Studies: A Reference Table for Clinicians (Abbassi-Ghanavati *et al.*, 2009).

Histological analysis of iron deposition by Prussian Blue staining

To detect $Fe^{3+,}$ samples were embedded in paraffin and sectioned at a thickness of 4 µm using a Leica RM2135 Microtome (Leica Biosystems, Germany). Fixed slides were dewaxed in a series of xylene and ethanol submersions and then washed in MilliQ water. A subset of collected placental villous tissue slides (Control n=7 and FGR n=7; : <3rd n=3, <5th n=2, <10th n=2) were stained with 10% (weight/weight) Prussian Blue (potassium hexacyanoferrate (II) trihydrate, Sigma-Aldrich, AUS) for 5 minutes, then 5% (weight/weight) Prussian Blue stain in 10% HCl for 30 minutes, and counterstained with nuclear fast red for 5 minutes (Sigma Aldrich, AUS) as described by Zaugg *et al.* (2024). Slides were then washed and dehydrated following gradient ethanol exposure of 70% and 100% for 3 minutes, finishing with a 10-minute xylene exposure. Slides were mounted with a coverslip and left to dry overnight. Slides were then imaged on Aperio GT 450 DX (Leica Biosystems, Germany) at 40X magnification. The intensity of the Prussian blue staining was quantified using H-scores obtained from Halo

205 Quantitative Pathology analysis software (Indica Labs; USA). All images were processed using
206 identical parameters to ensure valid comparisons between healthy and FGR placental samples.
207
208 *Placental RNA Preparation and Gene Expression Studies*
209 Placental tissue was crushed on dry ice with liquid nitrogen and subsequently, lysed and
210 homogenised with 1 mL Trizol® Reagent (Life Technologies; Thermo Fisher Scientific, AUS)
211 using the Precellys24 instrument (Bertin Technologies, France) for two cycles of 30 seconds at
212 5000 × g, incubated on ice for 30 minutes, and then repeated. Samples were centrifuged for 10
213 minutes at 10,000 × g using the Microfuge 20R (Beckman Coulter, AUS). The remainder of
214 the protocol was performed in line with the manufacturer's instructions outlined in the Direct-
215 zol™ RNA mini-prep kit (Zymo Research, California, USA). Following quantification on the
216 Nanodrop One (Thermo Scientific, AUS), 1000 ng of cDNA was synthesised using
217 SuperScript™ IV First-Strand Synthesis System (Thermo Fisher Scientific, AUS). RT-qPCR
218 was conducted using the PowerUpTM SYBR Green Master Mix (Applied Biosystems, Thermo
219 Fisher, AUS) with KiCqstart primers (Sigma Aldrich, AUS; Table 1). RT-qPCR was performed
220 using the QuantStudio6 Flex Real-Time PCR system (Thermo Fisher Scientific, MA, USA).
221 Relative gene expression was determined by normalising to the geometric mean of three
222 housekeeping genes (β-Actin, TBP, and YWHAZ), which were quantified using the $2^{-\Delta\Delta CT}$
223 method to assess relative gene expression within placental tissue samples.
224
225 **Table 1: Kicqstart Primers for Gene Expression Studies of Targeted Iron Transporters**
226 **and Intermediaries.**

Target Gene Name	**Gene Abbreviation**	**Primer sequence**
Cellular Iron Transporters		
Transferrin Receptor 1	TFRC	F 5'-AAGATTCAGGTCAAAGACAG-3' R 5'-CTTACTATACGCCACATAACC-3'
Solute Carrier Family 11 Member 2	SLC11A2	F5'-GAGTATGTTACAGTGAAACCC-3' R 5'-GACTTGACTAAGGCAGAATG-3'
Solute Carrier Family 40 Member 1	SLC40A1	F 5'-AAAGATACTGAGCCAAAACC-3' R 5'-GTTGTAGTAGGAGACCCATC-3'
Mitochondrial Iron transporters		
Solute Carrier Family 25 Member 37/ Mitoferrin 1	SLC25A37	F 5'-GGTAATGAATCCAGCAGAAG-3' R 5'-AGGAACTCATAGGTGATGAAG-3'

Solute Carrier Family 25 Member 28/ Mitoferrin 2	SLC25A28	F 5’-ACCTTTGATAACCTCTCTCC-3’ R 5’-TATTAGGAACCAGGGGAATG-3’
Mitochondrial Heme Synthesis		
Coproporphyrinogen Oxidase	CPOX	F 5’-CATGGAAATCTTTCAGAGGAAG-3’ R 5’-ATTCTTGGGGTGGATAACAG-3’
Ferrochelatase	FECH	F 5’-GGAAGAATATCCTCTTGGTTC-3’ R 5’-CACTCCTTGGCTAAAACTTG-3’
Erythropoiesis		
Hemogen	HEMGN	F 5’-CAAGATGGATTTGGGAAAGG-3’ R 5’-TCTGGAGAATGGTTCTCTTC-3’
Haemoglobin Subunit Alpha	HBA	F 5’-GACCTCCAAATACCGTTAAG-3’ R 5’-ACTTTATTCAAAGACCACGG-3’
Haemoglobin Subunit Beta	HBB	F 5’-ATTTGCTTCTGACACAACTG-3' R 5’-CAAAGGACTCAAAGAACCTC-3’
Haemoglobin Subunit Gamma 1	HBG1	F 5’-ACTTCCTTGGGAGATGCCAC-3’ R 5’-GCCTATCCTTGAAAGCTCTGA-3’
Haemoglobin Subunit Gamma 2	HBG2	F 5’-ACTTCCTTGGGAGATGCCAT-3’ R 5’-GCCTATCCTTGAAAGCTCTGC-3’
Erythrocyte Membrane Protein Band 4.1	EPB41	F 5’-AAAGGACTTGGAAGGAGTAG-3’ R 5’-GCGGTTAATTCTCAGCTTATC-3’
Solute Carrier Family 4 Member 1	SLC4A1	F 5’-CAAGAACAGCTCCTATTTCC-3' R 5’-CTGAATGAAGAAATCCACCAG-3'
Iron-Sulfur Cluster biosynthesis		
LYR Motif Containing 4	LYRM4/ISD11	F 5’-AGGATAAGAGATGCCTTCAG-3’ R 5’-ATCTGTCGACGAATTACTCC-3’
NADH: Ubiquinone Oxidoreductase Subunit AB1	NDUFAB1	F 5’-CAGGTTCCTTGGTAGAGTTAC-3’ R 5’-TGGGTCAATCTTGTCATAGAG-3’
Ferredoxin 2	FDX1L/FDX2	F 5’-CATGTGTATGTGAGTGAAGAC-3’ R 5’-TAGAAGGTTCCTGGTGATCTTG-3’
Frataxin	FXN	F 5’- GAAAGACTAGCAGAGGAAAC-3’ R 5’-TCCCAAAGGAGACATCATAG-3’

Iron-Sulfur Cluster Assembly Enzyme	ISCU	F 5'- GTGTAGACCTTTCTGCTCAGG-3' R 5'-TAGATGTCTTGTCAAGGGAC-3'
Glutaredoxin 5	GLRX5	F 5'-AAGAAGGACAAGGTGGTG-3' R 5'-TAGTCTTTAATGCCTTGTCG-3'
The NFU1 Iron-Sulfur Cluster Scaffold	NFU1	F 5'-CCCTAGTTCAATCATTACTCTG -3' R 5'-CATCATCCATAACCTGTTCTAC- 3'
NUBP Iron-Sulfur Cluster Assembly Factor	NUBPL	F 5'-TGAAGTTCTAGGAGACATTCC-3' R 5'-TCTTCTTACCACTTCCACAG-3'
BolA Family Member 3	BolA3	F 5'-CGAGCTACAGCTATAAAAGTC-3' R 5'-TTGGGGACAGAGGTAAATATC-3'
Housekeeper Genes		
Beta Actin	β-Actin	F 5'-GACGACATGGAGAAAATCTG-3' R 5'-ATGATCTGGGTCATCTTCTC-3'
Tryptophan 5-Monooxygenase Activation Protein Zeta	YWHAZ	F 5'-CCTGCATGAAGTCTGTAACTGAG-3' R 5'-GACCTACGGGCTCCTACAACA-3'
TATA-Box Binding Protein	TBP	F 5'-GCCAAGAGTGAAGAACAG-3' R 5'-GAAGTCCAAGAACTTAGCTG-3′

KiCqStart Primers targeting nuclear DNA involved in placental transport and iron-dependent pathways. Forward (F) and Reverse (R) primers were reconstituted to a 100 µM final concentration following the manufacturer's instructions. Gene expression was analysed using the $2^{-\Delta\Delta CT}$. Genes were examined in response to the physiological function of Iron in healthy and FGR placentae.

Proteomics Studies:

Placental tissue was crushed on dry ice and stored at -80°C until Liquid Chromatography-Mass Spectrometry (LC-MS) based proteomic analysis could be performed. LC-MS sample preparation followed previously published methodology by Mulhall *et al.* (2024), with placental tissue samples lysed in chilled 4% (weight/volume) sodium deoxycholate (SDC), 100 mM Tris HCl (pH.8.5) and passed through an 18G blunt-end needle before sonification. Samples were quantified and concentrations equalised to 200 µg/µl before digestion, alkylation and overnight trypsin incubation. Following trypsin exposure, peptides were diluted 1:1 with 100 mM Tris-HCl (ensuring SDC concentration < 1%) and vortexed briefly before adding 99% ethylacetate /1% Trifluoroacetic acid (TFA; 1:1) and thoroughly vortexed at 2000 rpm using

243 ThermoMixer. Peptides were then desalted using styrene-divinylbenzene reverse-phase
244 sulfonated StageTips.
245
246 Peptide separation was performed on an Aurora Ultimate C18 column (25 cm × 75µm,
247 IonOpticks) using a 90-minute linear gradient from 3% to 41% of solvent B (acetonitrile in
248 0.1% formic acid) at a flow rate of 400 nL/min. MS analysis was conducted on an Eclipse mass
249 spectrometer (Thermo Fisher Scientific, AUS), and MS scans were acquired over a mass range
250 of 375-1400 m/z at a resolution of 60,000, with an automatic gain control (AGC) target of
251 100% and maximum injection time of 50 ms. MS/MS scans were acquired at a resolution of
252 15,000, with an AGC target of 100%, normalised collision energy of 30%, and dynamic
253 maximum injection time. Raw data was analysed using Proteome Discoverer 2.5 (Thermo
254 Fisher Scientific, AUS), outlined by Murray *et al.* (2023).
255
256 *Western Blotting*
257 To validate our proteomics data, western blotting was performed. Protein was extracted from
258 healthy (n=7) and FGR (n=7) placental tissue using 1 mL RIPA buffer (50 nM Tris-HCl (pH
259 7.4), 150 nM NaCl, 1% NP-P40, 1% sodium deoxycholate, 1% SDS, Complete Mini Protease
260 Inhibitor Cocktail tablets (Roche Diagnostics, North Ryde AUS) and 1 nM PMFS). Samples
261 were homogenised using Precellys24 and centrifuged as outlined previously. The supernatant
262 was collected and stored at -80°C for subsequent western blotting analysis. Following Fisher
263 *et al.* (2019) published protocol, samples (40 µg/µL) were loaded onto 12% Tris gels
264 (Invitrogen, AUS), electrophoresed, and transferred to Polyvinylidene fluoride (PVDF)
265 membranes. Membranes were blocked with Odyssey Intercept buffer (LICORBio, USA) for 1
266 hour, then incubated overnight with primary antibody, LYMR4 at 1:250 dilution (ab253001,
267 Abcam, AUS) and Beta Actin (ab8226, Abcam, AUS) at a 1:1000 dilution. After washing with
268 PBST, membranes were incubated for 1 hour with secondary antibodies anti-mouse
269 IRDye®800CW and anti-rabbit IRDye®680LT (LICORBio, USA) at 1:20,000 dilution and
270 washed with PBST. Membranes were imaged using the LI-COR Odyssey M system
271 (LICORBio, USA) and analysed with Studio Image v5.2.
272
273 *Assessment of Heme*
274 Placental heme concentrations were measured using a Heme Assay kit (MAK316, Sigma
275 Aldrich, AUS). Following the manufacturing instructions, a total of 250 µL of water was added
276 to a 96-well plate, creating a blank well. A standard well was created by mixing 50 µL of heme
277 calibrator and 200 µL of water. Subsequently, 50 µL of homogenised term and FGR samples

suspended in glycerol buffer (50 mM Tris HCl, 1 mM EDTA, 0.5% Glycerol) was mixed with 200 µL of reagent respectively. The plate was left to incubate for 5 mins at room temperature, and the absorbance of well contents was determined at 400 nm. All samples and standards were performed in duplicate, and total heme concentration was determined using the following equation:

$$[\text{Total Heme}]\left(\frac{\mu\text{mol}}{\text{L}}\right) = \frac{(\text{ODsample} - \text{ODblank})}{(\text{ODcalibrator} - \text{ODblank})} \text{ x } 62.5\left(\frac{\mu\text{mol}}{\text{L}}\right)$$

Statistical Analysis

All data were analysed using GraphPad Prism 10.0. Outliers were identified and removed using Grubbs and ROUT tests, and data normality was assessed using the Shapiro-Wilk test. For normally distributed data, student t-tests were performed. For data that did not follow a normal distribution, Welch t-tests were conducted. Statistical significance was set at $p < 0.05$. John Hunter Hospital clinical data are presented with 95% confidence intervals (CI) and interquartile ranges (IQR). Gene expression data were presented as mean ± standard error of the mean (SEM), and histological H-scores, accounting for blue-stained iron deposits within placental tissue, were quantified using Halo Quantitative Pathology Analysis Software (Indica Labs, USA) and calculated using the following formula (Wen *et al.*, 2024):

$$\text{Hscore} = (3 \times \%\text{ heavily stained}) + (2 \times \%\text{ moderately stained}) + (1 \times \%\text{ lightly stained})$$

This formula weights the staining intensity, generating a composite score ranging from 0-300, reflecting both the extent and intensity of iron deposits. Proteomic analysis was expressed as $\log_2$-fold change (FC) to determine differential protein expression between healthy controls and FGR, visualised using heatmaps. The $\log_2$-fold was derived from the ratio between healthy term placentae to assess changes in FGR placentae, so a positive $\log_2$-FC indicates higher protein abundance in healthy control placentae, whereas a negative $\log_2$-FC indicates higher protein abundance in FGR placentae. Peptides with fewer than 2 Peptide Spectrum Matches (PSMs) were excluded from the analysis.

Results

Clinical Insights into Maternal Iron Bioavailability, Birth and Gestational Characteristics

To better understand the potential role of iron throughout gestation, we evaluated clinical characteristics encompassing maternal physical attributes, birth-related factors, and gestational characteristics (Table 2). Analysis included maternal parameters (age and BMI), birth outcomes (gestational age at delivery, birth weight, birth centile, placental weight, fetal sex, mode of

delivery) and fetal biometry measurements following sonography assessment (estimated fetal weight (EFW%), abdominal circumference, femur length, head circumference, and amniotic fluid volume). FGR babies were significantly smaller ($p<0.0001$), with a median birth weight of 2415g (95% CI: 1760g-2356g), compared to healthy term babies, who had a median birth weight of 3555g (95% CI: 3346g- 3676g). Additionally, FGR babies had smaller placentae ($p<0.0001$), with a median placental weight of 556g (95% CI: 395g-519g), compared to healthy term babies, who had a median placental weight of 689g (95% CI: 628g-757g). Furthermore, fetal biometric measurements, including abdominal circumference ($p<0.0001$), femur length ($p=0.002$), and head circumference ($p=0.0007$), were all significantly lower in FGR pregnancies. Although the difference in amniotic fluid volume was not statistically significant, FGR pregnancies had lower amniotic fluid volume ($p=0.054$) compared to healthy term controls.

Maternal haematological indices and maternal haematocrit and anaemia screening (Table 2) were performed on healthy and FGR pregnancies. No clinical or statistical significance was observed between FGR and healthy control groups in haemoglobin (Hb), mean corpuscular haemoglobin (MCH), mean corpuscular haemoglobin concentration (MCHC), mean corpuscular volume (MCV), red cell count (RCC), hematocrit (HCt), systemic iron levels and transferrin (Tf). Maternal ferritin levels were higher ($p=0.029$) and red cell distribution width (RDW) lower ($p=0.006$) in FGR cases compared to healthy control, however, both parameters fell within clinical reference ranges.

Table 2: Maternal, Fetal and Birth Clinical Characteristics from Pregnancies Diagnosed as FGR And Healthy Term Controls.

	Term Control	**FGR**	**P value**
n	19	18	
a. Maternal and Birth Characteristics			
Maternal Age (years)	31 (27.8, 33.0)	28.5 (26.9, 31.0)	0.3631
Maternal Body mass index; BMI (kg/m^2)	26.0 (24.2, 28.2)	25.0 (22.4, 30.6)	0.8836
Birth weight (g)	3555 (3346, 3676)	2415 (1760, 2356)	**< 0.0001**

Placental weight (g)	689 (628,757)	556 (395, 519)	**< 0.0001**
Sex ratio	9 Males, 10 Females	8 Males, 10 Females	-
b. Fetal Biometry Measurements following Sonography Assessment			
Fetal abdominal circumference (mm)	330 (321, 339)	275 (257, 293)	**< 0.0001**
Fetal Femur Length (mm)	68.4 (66.3, 73.6)	61.6 (58.0, 65.2)	**0.002**
Fetal Head Circumference (mm)	328.0 (315.2, 347.6)	295.5 (282.4, 307.8)	**0.0007**
Amniotic Fluid Volume (cm)	12.6 (10.8, 15.4)	10.9 (7.99, 12.1)	0.054
UAD Pulsatility Index	0.950 (0.820,1.50)	1.10 (0.860, 1.41)	0.823
UAD Resistance Index	0.585 (0.530, 0.790)	0.620 (0.560, 0.730)	0.5476
c. Maternal Haematological Parameters			
Haemoglobin (Hb) *RI: 10.5-15.0g/dL*	12.7 (12.1, 13.0)	12.2 (11.8,12.7)	0.325
Mean Corpuscular Haemoglobin (mcH) *RI: 29.0-33.0pg/cell*	30.0 (28.4, 30.4)	30.0 (28.9, 30.8)	0.519
Mean Corpuscular Haemoglobin concentration (mcHc) *RI:310-360g/L*	345 (338, 352)	344 (338, 346)	0.437
Haematocrit (HCt) *RI: 38.0-41.0%*	37.6 (36.1,39.5)	37.1 (35.9, 38.7)	0.620
Mean Corpuscular volume (McV) *RI: 81-99 (μm^3)*	88.0 (86.1, 90.0)	88.0 (86.4, 90.4)	0.8
Red Cell Count (RCC) *RI: 2.81-4.55 $10^6/mm^3$*	4.09 (4.02, 4.34)	4.00 (3.86, 4.13)	0.081
Red Cell Distribution Width (RDW)	14.2 (13.8, 15.0)	13.4 (13.1, 13.7)	**0.006**

RI: 12.5-15.3%			
d. Maternal Haematocrit and Anaemia Screening			
Iron (Fe) *RI: 5.37-34.55µmol/L*	22.0 (14.5, 24.4)	15.50 (12.1, 20.4)	0.29
Transferrin (Tf) *RI: 2.2-5.3g/dL*	3.50 (2.97, 4.12)	3.20 (2.82, 3.76)	0.513
Ferritin (F) *RI: 30-200µg/L*	20.0 (14.8, 33.3)	46.0 (25.4, 67.7)	**0.029**

This table presents data from consenting participants at John Hunter Hospital. Data are presented as median and interquartile range (IQR). Shapiro-Wilk normality tests were conducted, with student t-tests or Welch's tests used where appropriate. Statistically significant values ($p<0.05$). Missing data are indicated by –.

Placental Iron Transport

Analysis of iron transporters between FGR and control placentae revealed significant alterations in gene expression and protein levels of iron import and export components. Transferrin Receptor 1 (TFRC) showed significantly increased mRNA expression ($p<0.005$, Figure 1A) and upregulated protein levels (-0.117 $\log_2$-FC; Figure 1D) in FGR placentae compared to healthy term placentae. Divalent Metal Transporter 1 (DMT1/SLC11A2) exhibited significantly increased mRNA expression in FGR ($p<0.05$, Figure 1B) compared with controls. In contrast, Ferroportin (FPN/SLC40A1; Figure 1C), the iron receptor responsible for transporting iron out of the placenta into fetal circulation, showed no significant difference in mRNA expression between FGR and healthy controls. FPN protein analysis (Figure 1D) revealed lower protein levels (0.646 $\log_2$-FC) in FGR placental villous tissue. These findings suggest FGR placentae are retaining iron for placental function. Following the clinical characterisation of maternal iron parameters and mRNA expression of iron transport into the placenta, the placental iron content between healthy and FGR placentae was assessed. Histological analysis by Prussian blue staining revealed intense blue regions with no statistical difference between healthy control (Figure 1F-H) and FGR (Figure 1I-K) placentae.

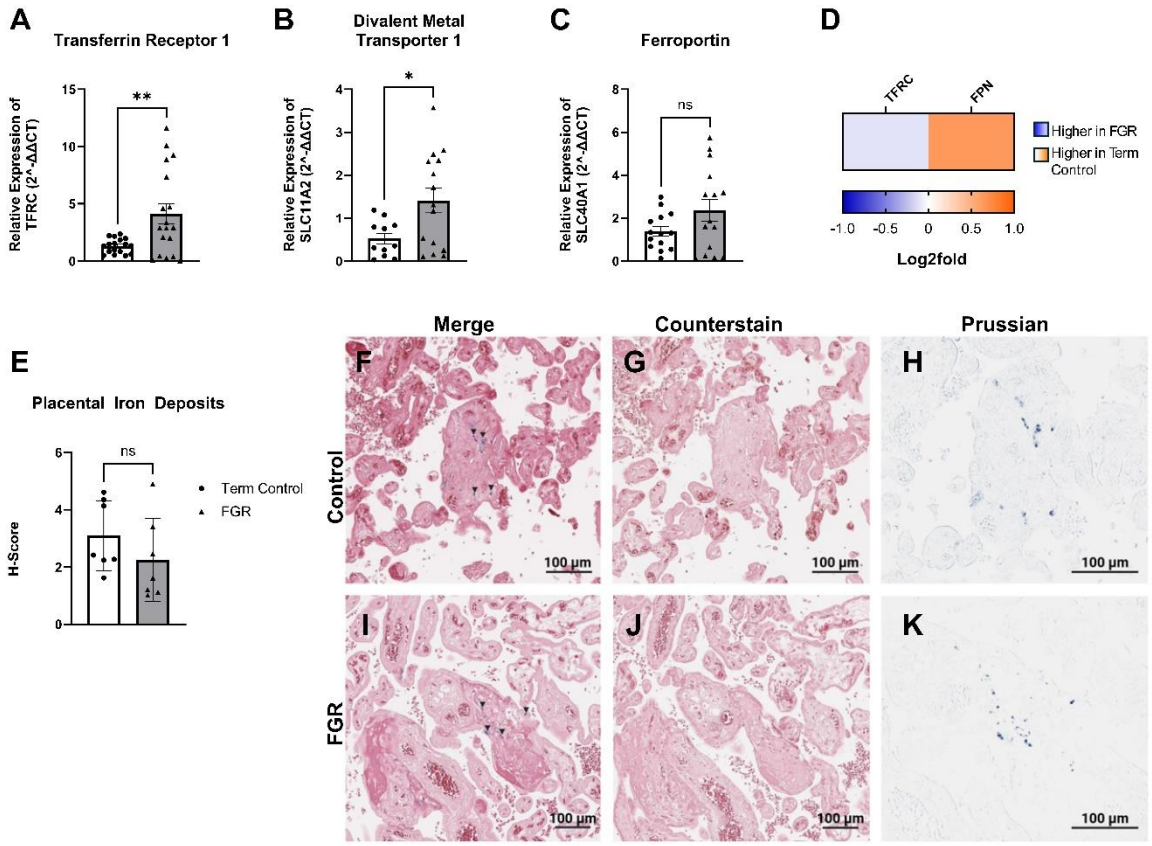

Figure 1: mRNA expression and protein levels of cellular iron transporters and histological Prussian blue staining in FGR and healthy control placental villous tissue. (A) TFRC, Transferrin Receptor 1; (B) SLC11A2, Solute Carrier Family 11 Member 2/ Divalent Metal Transporter 1 (DMT1); (C) SLC40A1, Solute Carrier Family 40 Member 1/Ferroportin (FPN). Data presented as mean ± SEM, control n=11-19 (white and circles), FGR n=10-18 (grey and triangles). Student t-tests were performed, *p<0.05, **p<0.01, ***p<0.001, ****p<0.0001. (D) Proteomes of cellular iron transport depicted as a heatmap based on the log2fold, with transporters indicated on top. The $\log_2$-FC was derived from the ratio between healthy term placentae to assess changes in FGR placentae, so a positive $\log_2$-FC indicates higher protein abundance in healthy control placentae (orange), and a negative $\log_2$-FC indicates higher protein abundance in FGR placentae (blue). (E) Halo Pathology Analysis Software was used to quantify the percentage of Prussian blue staining relative to the tissue area. Heavy, moderate, and light intensity values were used to calculate the H-score in healthy control (n=7) and FGR (n=7) placental tissue. An unpaired t-test revealed no significant difference between the groups. (F) A representative merged image of healthy control placental tissue showing Fe^{3+} deposits (blue staining indicated by arrows). (G) Control placental tissue stained with nuclear fast red counterstain only and (H) Prussian blue staining isolated from

375 counterstained tissue in (F), upon which intensity calculations were performed. (I) A
376 representative merged image of FGR placental tissue, with (J-K) shown similarly to the row
377 above (G-H). The scale bar represents 100µm.
378
379 *Mitochondrial Iron Transport*
380 Given the pivotal role of iron in mitochondrial function, we examined mitochondrial iron
381 transporters located within the inner mitochondrial membrane, Mitoferrin 1 (Solute Carrier
382 Family 25 Member 37, SLC25A37) and Mitoferrin 2 (Solute Carrier Family 25 Member 28,
383 SLC25A28). No significant difference in mitoferrin 1 (Figure 2A) mRNA expression was
384 observed in FGR placentae compared to healthy controls. In contrast, mitoferrin 2 (Figure 2B;
385 $p<0.005$) mRNA expression was significantly lower in FGR placental villous tissue than in
386 healthy controls.
387
388 *Mitochondrial Iron Utilisation: De Novo Fe-S Cluster Synthesis*
389 The utilisation of iron within the mitochondria converges on the synthesis of Fe-S clusters.
390 This process comprises two main stages: de novo synthesis of [2Fe-2S] clusters and late-stage
391 genesis of [4Fe-4S] clusters vital to mitochondrial function and cellular viability. In de novo
392 Fe-S cluster synthesis, the mRNA expression of LYR Motif 4 (LYRM4/ISD11; Figure 2C),
393 NADH: Ubiquinone Oxidoreductase Subunit AB1 (NDUFAB1/ACP; Figure 2D) and Frataxin
394 (FXN; Figure 2E) were similar in FGR and healthy control placental villous tissue. Conversely,
395 protein levels of NDUFAB1 (0.123 $\log_2$-FC; Figure 2L) were lower in FGR placentae
396 compared with healthy controls. Ferredoxin 2 (FDX2/FDX1L) mRNA expression (Figure 2G)
397 was significantly lower ($p<0.05$), while ferredoxin reductase (FDXR; Figure 2L) was 1.08 $\log_2$-
398 fold lower in protein levels in FGR compared to controls. The mRNA expression of Iron-Sulfur
399 Cluster Assembly Scaffold Enzyme (ISCU; Figure 2F), which is essential for [2Fe-2S]
400 assembly and transfer, was significantly lower ($p<0.05$) within FGR placental tissue compared
401 with healthy controls. However, ISCU protein expression (-0.372 $\log_2$-FC; Figure 2L) was
402 higher in FGR placental villous tissue when compared with healthy controls. An important
403 transporter of the [2Fe-2S] cluster, Glutaredoxin 5 (GLRX5; Figure 2H), had significantly
404 lower mRNA expression ($p<0.05$) in FGR placentae; however, no difference in protein
405 abundance between FGR and healthy term placentae was observed.
406
407 *Late-Stage Fe-S Cluster Synthesis*
408 In late-stage Fe-S cluster assembly, Heat Shock Protein Family A (HSP70) Member 9 (HSPA9;
409 Figure 2L) observed a 0.219 $\log_2$-fold increase at the protein level in healthy controls compared

410 to FGR placentae. IBA57 (Figure 2L) was -0.073 $\log_2$-fold higher in protein level with
411 statistical significance ($p<0.005$) confirmed by western blotting (Figure 2M). [4Fe-4S] cluster
412 transporters showed increased mRNA expression of NFU1 Iron-Sulfur Cluster Scaffold
413 (NFU1; $p<0.005$, Figure 2I) and BOLA Family member 3 (BOLA3; $p<0.05$, Figure 2J) in FGR
414 placental villous tissue when compared to healthy controls. No significant changes in mRNA
415 expression were observed in NUBP Iron-Sulfur Cluster Assembly factor (NUBPL; Figure 2K).

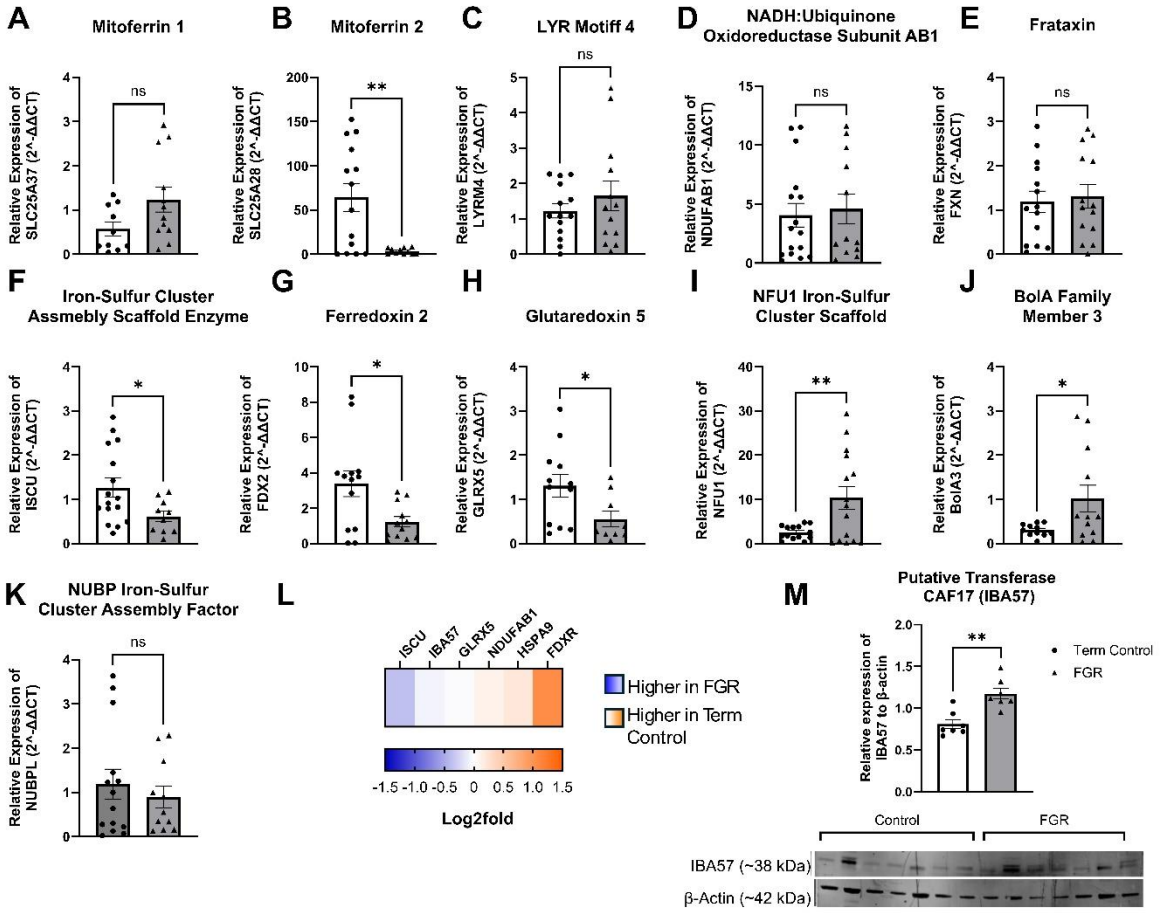

416

417 **Figure 2: mRNA expression and proteomes of targeted genes in the iron-sulfur (Fe-S)**
418 **cluster biosynthesis pathway.** (A) SLC25A37, Solute Carrier Family 25 Member 37/
419 Mitoferrin 1; (B) SLC25A28, Solute Carrier Family 25 Member 28/Mitoferrin 2 (C) LYRM4,
420 LYR Motif Containing 4 (ISD11); (D) NDUFAB1, NADH: Ubiquinone Oxidoreductase
421 Subunit AB1; (E) ISCU, Iron-Sulfur Cluster Assembly Enzyme; (F) FXN, Frataxin; (G)
422 FDX1l, Ferredoxin 2 (FDX2); (H) GLRX5, Glutaredoxin 5; (I) NUBPL, NUBP Iron-Sulfur
423 Cluster Assembly Factor; (J) NFU1, NFU1 Iron-Sulfur Cluster Scaffold; (K) BolA3, BolA
424 Family Member 3; Data are presented as mean ± SEM, control n=11-19 (white and circles),
425 FGR n=10-18 (grey and triangles). Student t-tests were performed *$p<0.05$, **$p<0.01$,
426 ***$p<0.001$, ****$p<0.0001$. (L) Fe-S cluster proteomes, depicted as a heatmap based on $\log_2$-

FC with proteome identification on top. Proteomes of Fe-S cluster assembly depicted as a heatmap based on the log_2-FC, with transporters indicated on top. The log_2-FC was derived from the ratio between healthy term placentae to assess changes in FGR placentae, so a positive log_2-FC indicates higher protein abundance in healthy control placentae (orange), and a negative log_2-FC indicates higher protein abundance in FGR placentae (blue). (M) Protein abundance of putative transferase CAF17 (IBA57; 38.155kDa) normalised to β-Actin (41.737kDa) in healthy and FGR placentae. Representative immunoblot shown below.

Heme Synthesis

Analysis of the heme synthesis pathway showed significantly higher mRNA expression of coproporphyrinogen oxidase (CPOX; p=0.002; Figure 3A) and ferrochelatase (FECH; p=0.005; Figure 3B) at the gene and protein level, -0.163 log_2-fold and -0.356 log_2-fold, respectively (Figure 3D) within FGR placental tissue compared to healthy tissue. Furthermore, protein levels of additional enzymes important to heme synthesis, Uroporphyrinogen Decarboxylase (UROD; Figure 3D) Hydroxymethylbilane Synthase (HMBS; Figure 3D), were -0.175 log_2-fold and -0.196 log_2-fold greater in FGR, respectively. In contrast, Aminolevulinate dehydratase (ALAD/PBGS; Figure 3D) was 0.541 log_2-fold lower protein expression in FGR compared with term control placental villous tissue. Although heme synthesis enzymes were upregulated, this was not conserved when assessing heme activity (p<0.005) in FGR placentae. Heme oxygenase (HMOX) -1 protein abundance was -1.13 log_2-fold higher in FGR placentae compared to control placentae (Figure 3D). Additionally, NADPH-cytochrome P450 oxidoreductase (POR) protein abundance was -0.157 log_2-fold higher in FGR placentae than healthy controls.

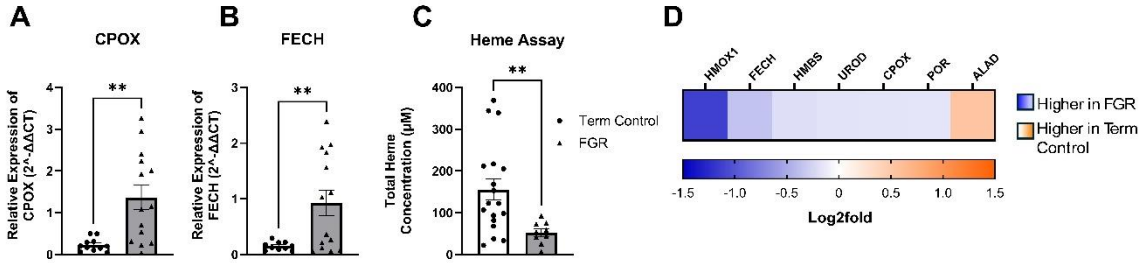

Figure 3: mRNA expression of targeted genes involved in the heme synthesis pathway and heme content in FGR and healthy term placentae. (A) CPOX, Coproporphyrinogen Oxidase; (B) FECH, Ferrochelatase. Data presented as mean ± SEM, control n=11-19 (white and circles), FGR n=10-18 (grey and triangles), with sample loss due to outliers' tests conducted. Student t-tests were performed *p<0.05, **p<0.01, ***p<0.001, ****p<0.0001.

456 (C) Heme Assay measuring total Heme Concentration (μM) present. (D) Heme synthesis
457 proteomes depicted as a heatmap based on log_2-FC, with proteome identification on top.
458 Proteomes of heme synthesis depicted as a heatmap based on log_2-FC, with transporters
459 indicated on top. The log_2-FC was derived from the ratio between healthy term placentae to
460 assess changes in FGR placentae, so a positive log_2-FC indicates higher protein abundance in
461 healthy control placentae (orange), and a negative log_2-FC indicates higher protein abundance
462 in FGR placentae (blue).
463
464 The placenta is a potent haemopoietic site where heme synthesis stimulates globin production,
465 forming a haemoglobin tetramer of alpha and beta-like chains critical for binding and
466 transporting oxygen. Our analysis revealed no changes in the mRNA expression of
467 Haemoglobin Subunit Alpha 1 (HBA1) between controls and FGR placental villous tissue,
468 although protein levels were 0.210 log_2-fold lower in FGR compared to healthy controls
469 (Figure 4A and G). Within the beta-like globin chains, we observed significantly greater mRNA
470 expression of Haemoglobin Subunit Gamma 1 (HBG1; $p<0.05$, Figure 4B) in FGR placentae,
471 although Haemoglobin Subunit Gamma 2 showed no differences between control and FGR
472 placentae. Protein abundance of HBG1 (0.325 log_2-FC) and HBG2 (0.092 log_2-FC) was lower
473 in FGR compared with term control placental tissue samples (Figure 4G). Haemoglobin
474 Subunit Beta (HBB) mRNA expression was significantly higher ($p<0.05$) in FGR compared to
475 healthy controls (Figure 4D). However, HBB protein abundance was lower (0.585 log_2-FC)
476 within FGR placental tissue when compared to healthy placental tissue samples (Figure 4G).
477 Levels of Erythrocyte structural proteins, specifically Erythrocyte Protein Band 4.1 (EPB41),
478 EPB42, Spectrin Alpha 1 (SPTA1), Spectrin Beta (SPTB), Ankyrin1 (ANK1) and Solute
479 Carrier Family 4 Member 1 (SLC4A1), were subsequently assessed. The mRNA expression
480 ($p<0.05$) and protein abundance (0.254 log_2-FC) of EPB41 were lower in FGR placental tissue
481 compared to healthy tissue controls (Figure 4E and G). EPB42 protein abundance was 0.562
482 log_2-fold lower within FGR placentae than healthy placentae (Figure 4G). Analysis of spectrin
483 protein levels, SPTA1 and SPTB (Figure 4G), was 0.156 log_2-fold and 0.491 log_2-fold lower
484 in FGR placenta compared with healthy term placenta. Similarly, ANK1 and SLC4A1 protein
485 abundance were 0.661 log_2-fold and 0.493 log_2-fold lower in FGR placentae than healthy
486 placentae, suggesting compromised erythrocyte structure. However, analysis of Hemogen
487 (HEMGN; Figure 4F), a regulator of haematopoietic cell differentiation, mRNA expression
488 was similar in healthy and FGR placental villous tissue, indicating that these changes were not
489 occurring at the onset of hematopoiesis but rather at erythrocyte maturation.

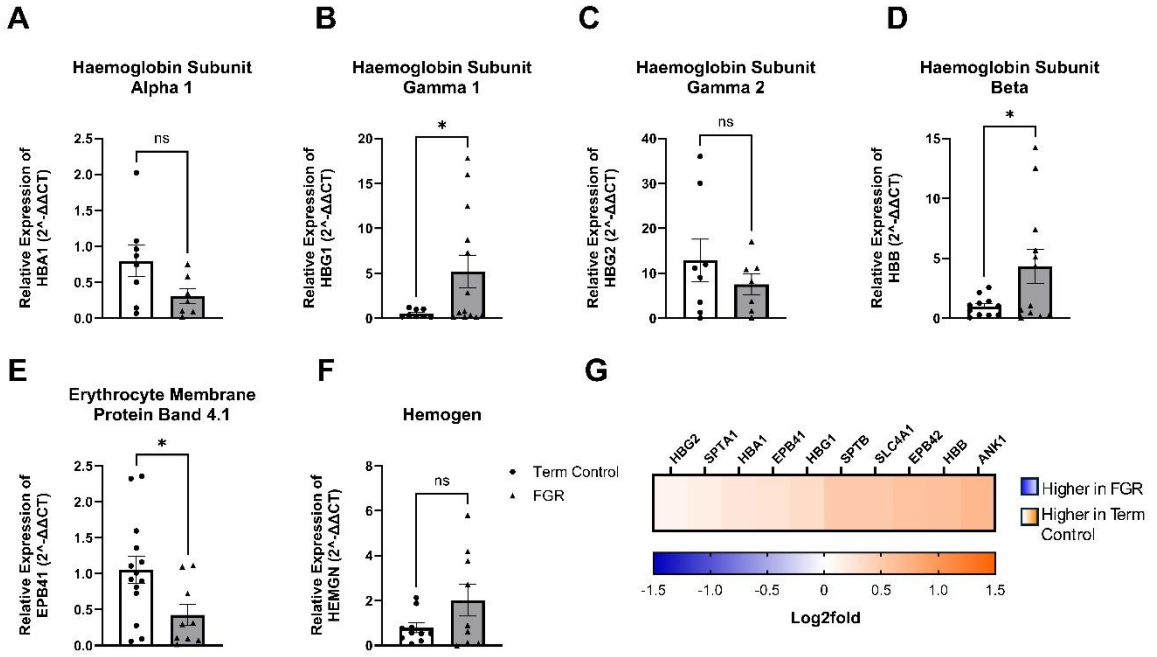

Figure 4: mRNA expression and proteome of targeted genes involved in Haematopoiesis. (A) HBA1. Haemoglobin Subunit Alpha 1; (B) HBG1, Haemoglobin Subunit Gamma 1; (C) HBG2, Haemoglobin Subunit Gamma 2; (D) HBB, Haemoglobin Subunit Beta; (E) EPB41, Erythrocyte Membrane Protein Band 4.1; (F) HEMGN, Hemogen; Data presented as mean ± SEM, control n=11-19 (white and circles), FGR n=10-18 (grey and triangles). Student t-tests test performed *p<0.05, **p<0.01, ***p<0.001, ****p<0.0001.(G) Haematopoiesis proteomes, depicted as a heatmap and based on log_2-FC with proteome identification on top. Proteomes of haematopoiesis depicted as a heatmap based on log_2-FC, with transporters indicated on top. The log_2-FC was derived from the ratio between healthy term placentae to assess changes in FGR placentae, so a positive log_2-FC indicates higher protein abundance in healthy control placentae (orange), and a negative log_2-FC indicates higher protein abundance in FGR placentae (blue).

Discussion

This project sought to elucidate the complex role of iron in placental and mitochondrial function in fetal growth restriction (FGR). As expected, we observed reduced placental and birth weights in FGR compared with healthy controls (Table 2). Similarly, fetal biometric measurements showed significantly reduced abdominal circumference, head circumference, and femur length in FGR pregnancies compared with healthy-term pregnancies. Mothers with FGR babies also showed reduced red cell distribution width (RDW) in conjunction with elevated ferritin levels, although these fell within clinical reference ranges. No changes were

observed in circulating maternal iron or haemoglobin levels, and all maternal measurements stayed within the clinical reference ranges (Table 2). Subsequent analysis of FGR placental tissue identified altered iron transporters (Figure 1). Furthermore, FGR placentae showed changes in mitochondrial iron-sulfur (Fe-S) cluster biosynthesis, specifically a reduced capacity for converting [2Fe-2S] to [4Fe-4S] clusters due to lower levels of key [2Fe-2S] proteins ferredoxin reductase (FDXR) and ferredoxin 2 (FDX2) required for synthesis of both [2Fe-2S] and late-stage [4Fe-4S] clusters (Figure 2). The observed reduction in proteins involved in [4Fe-4S] cluster assembly suggests a metabolic redirection from incorporation into the mitochondrial electron transport chain (ETC) toward increased heme production, as evidenced by increased cytosolic and mitochondrial proteins of the heme synthesis proteins (Figure 3). Despite the apparent shift toward heme synthesis, total heme concentrations in FGR placentae were decreased. We propose that this arises from increased regulation of the heme degradation pathway in FGR placentae, evidenced by elevated protein levels of heme oxygenases and NADPH-cytochrome P450 oxidoreductase. Consequently, we observed reduced haemoglobin proteins within the FGR placentae (Figure 4). Additionally, our findings identified alterations in levels of erythrocyte structural proteins in FGR placentae (Figure 4). These alterations may further compromise oxygen delivery to the fetus or simultaneously represent an adaptive response to the poor vasculature of FGR placentae. Together, these findings enhance our understanding of the fundamental biological processes underlying FGR and highlight how adaptations in iron utilisation contribute to mitochondrial dysfunction observed in FGR, perpetuating inadequate fetal growth.

Maternal Haematological Assessment in FGR

Pregnancy is a dynamic process that is associated with significant alterations in the maternal cardiovascular system to support fetoplacental development (Sanghavi & Rutherford, 2014). Maternal cardiovascular adaptations, including increased plasma volume (20-50%) and red blood cell mass (20-30%), begin rising from week 5 of pregnancy, well before the maternal and fetal circulatory systems are functionally established via the placenta (Allerkamp *et al.*, 2022; Mégier *et al.*, 2022; Söhnchen *et al.*, 2011). Additionally, studies have shown that erythropoiesis is the largest consumer of iron and as gestation advances, the demand for iron increases substantially to support expanded maternal red cell mass, placental development, and fetal growth (Gambling *et al.*, 2001; Kautz & Nemeth, 2014). Maternal cardiovascular function and haemodynamic failures have significant implications for the health of both the mother and the fetus.

547 In FGR pregnancies, normal maternal haemodynamic responses are known to be compromised,
548 including inadequate blood volume expansion and impaired reduction in vascular resistance
549 (Mecacci *et al.*, 2021; Perry *et al.*, 2020). Therefore, our study assessed whether maternal
550 haemodynamic responses in FGR pregnancies might be reflected in maternal blood parameters
551 (Table 2). We observed reduced maternal red blood cell distribution width (RDW) in FGR
552 mothers compared with controls. RDW is the measurement of variation in red blood cell size
553 and volume relative to the mean red cell volume (MCV) (Fava *et al.*, 2019; Shehata *et al.*,
554 1998). Despite being statistically significant, the reduction in maternal RDW remained within
555 clinical reference ranges, indicating decreased anisocytosis, less variability in erythrocyte size
556 and a narrower distribution around the mean cell volume (de Freitas *et al.*, 2019; Kurt *et al.*,
557 2015; Lippi & Plebani, 2014). We speculate that the statistical significance in maternal RDW
558 between FGR and healthy control mothers, while within clinical reference ranges, may be a
559 maternal adaptation to overcome poor spiral artery remodelling. Improved erythrocyte
560 uniformity may enhance blood rheology (Nader *et al.*, 2019; Reddy *et al.*, 2016; Zhang *et al.*,
561 2009), which may provide advantages in the context of increased vascular resistance and
562 narrowed maternal spiral arteries, contributing to the reduced perfusion of the intervillous space
563 often observed in FGR (Burton & Jauniaux, 2018).
564
565 Maternal serum ferritin levels were significantly higher in FGR pregnancies than in healthy
566 controls (Table 2), although ferritin levels fell within clinical reference ranges (30-200 μg/L).
567 Our observations are substantiated by previous studies showing that elevated serum ferritin
568 levels increased the risk of developing FGR (Ozgu-Erdinc *et al.*, 2014). Furthermore, Hou *et*
569 *al.* (2000) demonstrated that FGR pregnancies with elevated serum ferritin levels presented
570 with asymmetric fetal growth during the second and third trimesters. Asymmetrical growth is
571 a key hallmark of late-onset FGR (diagnosis >32 weeks), accounting for 70-80% of FGR cases
572 (Sun *et al.*, 2020). This may explain why serum ferritin levels were higher in FGR cases within
573 our study, as 83% of our samples were delivered >32 weeks. Moreover, serum ferritin's
574 specificity (true negative rate in identifying iron sufficiency) and sensitivity (true iron
575 deficiency) are essential for assessing biological iron status when chronic inflammation is
576 absent (Mégier *et al.*, 2022). The increase in maternal serum ferritin may, therefore, be
577 attributed to an inflammatory response as ferritin acts as an acute-phase reactant during
578 inflammation (Camaschella, 2015), rather than truly indicating maternal iron status, as
579 pregnancy is inherently pro-inflammatory. This is supported by increases in oxidative stress

and inflammation observed in the maternal circulation and placenta of FGR pregnancies (Hou *et al.*, 2000; Ozgu-Erdinc *et al.*, 2014).

Despite statistically elevated maternal serum ferritin levels and reduced RDW in FGR, the lack of maternal changes in iron haematological parameters, outside of normal reference ranges, suggests that subsequent findings were not due to impaired iron delivery but rather demonstrate that maternal adaptations are likely secondary responses to compromised placental function.

Iron transport in the FGR placenta.

Our study revealed that iron transporter proteins were altered in FGR placentae, characterised by an enhanced capacity for iron uptake. Specifically, we observed a 1.08-fold increase in Transferrin receptor 1 (TfR1/TFRC) levels (-0.117 log2-fold), the major importer of non-heme iron into cells, in FGR placenta (Figure 1A and D). While maternal iron deficiency has been shown to increase TfR1 expression in placental tissue, ensuring appropriate iron uptake from maternal circulation to support fetal and placental iron requirements, we found no evidence of maternal iron deficiency within our FGR group (Table 2). However, Burton and Fowden (2012) and Sibley *et al.* (2010) report that when placental size and capacity are reduced, the placenta increases nutrient transporter activity as a compensatory mechanism to suboptimal conditions, rather than failing. This may explain our observed increases in iron transporters in significantly smaller FGR placentae (Table 2). Collectively, this suggests that the increase in TfR1 in our FGR placentae might represent a compensatory response to maximise iron uptake in a compromised placental vascular environment.

Since iron transport is transcellular and unidirectional from mother to fetus, the placenta serves as the "gatekeeper" for iron transfer to the fetus (O'Brien, 2022; Roberts *et al.*, 2020). The fetus depends entirely on maternal iron transfer through the placenta, mediated by ferroportin (FPN), which exports iron into the fetal circulation (Figure 1C-D) (Sangkhae *et al.*, 2020). We observed 1.56-fold lower FPN (0.646 log2-fold) levels in FGR placental tissue, suggesting that the placenta is retaining iron for its own use (O'Brien, 2022; Sangkhae *et al.*, 2020). This is supported by an increase in divalent metal transporter 1 (DMT1/SLC11A2) mRNA expression, the transporter of iron into the cell cytoplasm following endocytosis of the TfR1-iron complex (Figure 1B). Subsequent Prussian blue staining showed no difference in iron deposit content for ferric (Fe^{3+}) iron between FGR and healthy controls. Collectively, these findings suggest that iron is being prioritised for intracellular function in FGR placentae, rather than for storage or being exported into fetal circulation.

Mitochondrial Iron Transport

The mitochondria utilise between ~20-50% of cellular iron (Qi *et al.*, 2023), facilitating integral mitochondrial function and bioenergetic pathways to support fetoplacental growth (Aye *et al.*, 2022; Paul *et al.*, 2017). Mitoferrin-1 (SLC25A39) and mitoferrin-2 (SLC25A28) facilitate iron transport across the inner mitochondrial membrane but exhibit different cell expression profiles and cell-specific functions (Figure 2A-B) (Ali *et al.*, 2022). We observed no changes in mitoferrin-1 mRNA expression between our groups. In line with published literature in mice and zebrafish haematopoietic tissue (liver, bone marrow, spleen, and yolk sac islands) and embryonic tissue that determined mitoferrin-1 is essential for erythroid development to meet the higher demand for mitochondrial iron to support heme production (Paradkar *et al.*, 2009; Shaw *et al.*, 2006). As the placenta is a potent haematopoietic tissue containing erythroid progenitors from as early as 6 weeks of gestation through to term (Gekas *et al.*, 2005; Robin *et al.*, 2009). We propose that the expression of mitoferrin-1 is likely conserved, attributed to the placenta's fundamental role as a haematopoietic organ, rather than solely as a facilitator of maternal-fetal exchange. This is further demonstrated by Shaw *et al.* (2006) who observed that knockout (KO) of mitoferrin-1 in murine models results in embryonic lethality at the initiation of definitive erythrocyte development.

In contrast to mitoferrin-1, which is predominantly expressed in erythroid tissue, and minimal expressed in other tissues (Ali *et al.*, 2022), Shaw *et al.* (2006) and Paradkar *et al.* (2009) found that mitoferrin-2 is ubiquitously expressed in non-erythroid tissue and is responsible for the iron import required for haemoproteins and Fe-S cluster synthesis (Ali *et al.*, 2022). Our study observed a decrease in mitoferrin-2 mRNA expression in placentae from FGR pregnancies. These findings highlight the complex regulation of iron transport in FGR placentae, suggesting a selective downregulation of mitoferrin-2 while preserving mitoferrin-1 iron uptake for haematopoietic use.

Altered Iron-Sulfur Cluster Biosynthesis Machinery in FGR Placental Mitochondria

Given that our data suggested a conservation of intracellular iron and altered mitochondrial iron uptake within FGR placentae, we went on to investigate iron-sulfur (Fe-S) cluster biosynthesis. Fe-S clusters are apoproteins essential for cellular activities, including heme and are directly incorporated into the mitochondrial electron transport chain (ETC) to support mitochondrial structure and function (Guan *et al.*, 2022; Voltarelli *et al.*, 2023). Fe-S assembly

is a complex process that can be categorised into two main components: (i) de novo synthesis of [2Fe-2S] cluster and (ii) late Fe-S ([4Fe-4S]) cluster synthesis (Figure 3). Disruptions in Fe-S biogenesis impair cellular and mitochondrial function, and have been shown in literature to lead to metabolic myopathies such as Friedreich's ataxia, sideroblastic anaemia, and ISCU myopathy (Lee *et al.*, 2011).

Mitochondrial De Novo Fe-S Synthesis in FGR

De novo Fe-S cluster synthesis is a complex series of reactions, initiated by the catalysis of a pyridoxal-phosphate, cysteine desulfurase NFS1 (Maio & Rouault, 2020). Stabilising the activity of NFS1, NADH: Ubiquinone Oxidoreductase Subunit AB1 (NDUFAB1) forms a heterodimer with LYR Motif Containing 4 (LYRM4), initiating Fe-S cluster synthesis via the complex NFS1:LYRM4:NDUFBA1 (Figure 2C-D) (Herrera *et al.*, 2019). Our data showed a 1.09-fold lower abundance of NDUFAB1 (0.123 $\log_2$-fold) in FGR placentae, despite the heterodimer conjugate LYRM4 mRNA expression remaining unchanged. The subsequent synthesis of the NFS1:LYRM4:NDUFBA1 complex results in the binding of the iron-sulfur cluster assembly enzyme (ISCU) and frataxin (FXN), forming a hetero-octamer that consists of two copies of the NFS1:LYRM4:NDUFBA1:FXN:ISCU complex (Figure 2C-F and L) (Maio & Rouault, 2020).

In our study, FXN mRNA expression remained unchanged between the two groups (Figure 2E), suggesting any deficits in Fe-S assembly likely occur downstream of initial FXN-mediated iron and sulfide delivery onto ISCU, as loss of FXN results in widespread depletion of Fe-containing proteins and attenuation of mitochondrial protein synthesis (Figure 2E) (Zhong *et al.*, 2023). We observed a decrease in ISCU mRNA, which provides the structural scaffold for [2Fe-2S] formation, in FGR placental mitochondria (Figure 2F). However, this observation was not conserved in our proteomics data, with a 1.29-fold higher protein abundance in FGR (-0.372 $\log_2$-FC; Figure 2L). In addition, key [2Fe-2S] proteins ferredoxin reductase (FDXR) and ferredoxin 2 (FDX2), which are required to supply electrons to complete [2Fe-2S] and [4Fe-4S] assembly, had 2.11-fold lower protein (1.08 $\log_2$-FC) and decreased gene expression ($p<0.05$) in FGR placentae, respectively. As we did not observe global suppression, we suggest the FGR placenta prioritises [2Fe-2S] biogenesis at the detriment of [4Fe-4S] cluster synthesis (Figure 2G and L). This is consistent with previous knockdown studies showing that loss of FDX2 globally disrupts mitochondrial Fe-S assembly, leading to dysregulated oxidative phosphorylation (OXPHOS) and reduced antioxidant production (Shi *et al.*, 2012).

685 Following [2Fe-2S] cluster formation, GLRX5 receives the [2Fe-2S] cluster from ISCU for
686 transport to apoproteins required for various cellular and mitochondrial functions (Paul *et al.*,
687 2017). We observed a significant decrease in mRNA expression of GLRX5, yet GLRX5 protein
688 abundance remained unchanged between the two groups (Figure 2H and L), again preserving
689 the capacity for [2Fe-2S] cluster transfer to downstream cellular and mitochondrial functions
690 such as heme synthesis or late-stage Fe-S cluster formation.
691
692 *Mitochondrial Late-Stage Fe-S Synthesis in FGR*
693 Given the changes observed in de novo synthesis, specifically reductions in protein abundance
694 of FDXR and mRNA expression of FDX2 and their sequential roles in electron transfer in the
695 formation of [2Fe-2S] and [4Fe-4S] clusters, we investigated late-stage Fe-S synthesis. In
696 contrast to de novo Fe-S cluster synthesis, late-stage [4Fe-4S] clusters are critical cofactors that
697 are incorporated into mitochondrial ETC complexes, and apoproteins such as iron-regulatory
698 proteins, and antioxidants (Maio & Rouault, 2020).
699
700 The formation of [4Fe-4S] clusters requires the transfer of [2Fe-2S] intermediaries to the A-
701 type scaffold proteins, Iron-Sulfur Cluster Assembly 1 and 2 (ISCA1 and ISCA2) in
702 conjugation with Iron-Sulfur Cluster Assembly Factor IBA57 (Melber *et al.*, 2016; Paul *et al.*,
703 2017). In FGR placentae, we observed a small 1.05-fold increase in IBA57 protein (-0.073
704 $\log_2$-FC; Figure 2L), which was confirmed by western blotting to be significant ($p<0.002$;
705 Figure 2M). However, we did not detect ISCA1 and ISCA2 at sufficient levels within our
706 proteomic analysis. Given that ISCA1 and ISCA2 are known to contain [2Fe-2S] clusters
707 (Beilschmidt *et al.*, 2017; Nasta *et al.*, 2019) but IBA57 does not contain [2Fe-2S] clusters
708 (Amick *et al.*, 2014; Dores-Silva *et al.*, 2015), the inability to detect sufficient levels of ISCA
709 proteins in FGR may suggest that the newly synthesised [2Fe-2S] clusters cannot be effectively
710 matured into [4Fe-4S] clusters.
711
712 Newly synthesised [4Fe-4S] clusters are released from the ISCA1:ISCA2:IBA57 complex by
713 a chaperone/co-chaperone system comprising heat shock protein family A (HSP 70) member 9
714 (HSPA9) and mitochondrial Fe-S Cluster co-chaperone (HSC20). HSPA9 protein abundance
715 was 1.16-fold lower in FGR placentae (0.219 $\log_2$-FC; Figure 2L). Following [4Fe-4S] cluster
716 release, HSPA9 mediates the transfer [4Fe-4S] clusters directly to apoproteins or through
717 targeting factors such as NFU1 Iron-Sulfur Cluster Scaffold (NFU1), BolA Family Member 3
718 (BOLA3) and NUBP Iron-Sulfur Cluster Assembly Factor (NUBPL) (Maio & Rouault, 2020;
719 Melber *et al.*, 2016; Zhong *et al.*, 2023). Incorporation of [4Fe-4S] into the mitochondrial ETC

complexes provides electron tunnelling through complexes I-IV, generating energy and a proton gradient crucial for ATP synthesis (Mostajabi Sarhangi & Matyushov, 2023; Vanlander & Van Coster, 2018). Despite increased mRNA expression of BOLA3 and NFU1 in FGR placentae (Figure 2I-J), we observed no changes in NUBPL mRNA expression (Figure 2K), which may suggest an attempt to maximise the delivery of a limited pool of [4Fe-4S] clusters.

Collectively, the reduced FDX2 mRNA expression and lower abundance of FDXR and HSPA9 suggest a bottleneck in mitochondrial Fe-S cluster biogenesis in the FGR placenta. While these proteins participate in both [2Fe-2S] and [4Fe-4S] cluster formation (Maio & Rouault, 2020), their decreased abundance in FGR likely prioritises the direction of limited resources toward essential [2Fe-2S] cluster formation, for heme synthesis (Shi *et al.*, 2012; Weiler *et al.*, 2020). This disruption in mitochondrial Fe-S assembly provides a molecular basis for the mitochondrial dysfunction observed in FGR placentae, characterised by impaired respiratory chain complex activity, altered ATP production, and increased oxidative stress (Holland *et al.*, 2017; Xu *et al.*, 2021).

Altered Heme Synthesis and Erythrocyte Structure in FGR Placentae: Implications for Fetal Oxygenation and Development

Based on our data showing prioritisation of [2Fe-2S] clusters in FGR placentae, we further investigated the heme synthesis pathway. Heme synthesis critically depends on the insertion of [2Fe-2S] clusters into ferrochelatase (FECH), the terminal enzyme of heme biosynthesis that resides within the mitochondria. The insertion of [2Fe-2S] clusters into FECH ensures its stability and activity for heme production (Al-Karadaghi *et al.*, 1997; Obi *et al.*, 2022). Our data revealed significantly higher levels of enzymes across the heme synthesis pathway in FGR placentae (Figure 3D). Specifically, elevated mRNA and protein levels of enzymes coproporphyrinogen oxidase (CPOX; 1.12-fold; -0.163 $\log_2$ FC) and FECH (1.28-fold; -0.356 $\log_2$-fold), located within the mitochondria, were accompanied by greater protein abundance of heme enzymes Hydroxymethylbilane Synthase (HMBS; 1.15-fold), and Uroporphyrinogen Decarboxylase (UROD: 1.13-fold). Supporting our suggestion that the FGR placentae prioritises [2Fe-2S] clusters and shifts utilisation towards heme synthesis. Additionally, FECH has been reported to be complexed to ATP Binding Cassette Subfamily B Member 10 (ABCB10), conferring stability to mitoferrin-1. This FECH-ABCB10 conjugation may explain why mitoferrin-1 expression remains conserved in FGR placentae despite reduced mitoferrin-2.

755 Beyond its role in oxygen transport and haemoglobin production, heme also contributes to
756 mitochondrial respiration by facilitating electron transfer and proton translocation within ETC
757 complexes II, III, and IV through its incorporation as heme a, b, and c moieties (Kim et al.,
758 2012). Despite the increased levels of heme synthesis enzymes, the assessment of heme
759 concentration in FGR placentae was lower (Figure 3C). This may be due to increased
760 incorporation of heme a, b and c into ETC complexes II, III and IV to increase mitochondrial
761 respiration resulting from a lack of [4Fe-4S] assembly, although this hypothesis requires
762 confirmation.
763
764 Alternatively, heme is a known pro-oxidant, inducing oxidative stress, and heme accumulation
765 can induce its catabolism via heme oxygenase 1 (HMOX1), degrading heme into carbon
766 monoxide, iron and biliverdin (Figure 3D). We observed 2.19-fold higher HMOX1 abundance
767 in FGR placentae, suggesting that despite upregulation of the heme biosynthesis pathway,
768 increased heme breakdown may reflect heightened oxidative stress or a compensatory
769 mechanism to regulate "free" heme levels. The catabolism of heme by the placenta is not well
770 understood (Liu et al., 2016), although Peoc'h et al. (2020) have suggested that HMOX
771 expression in the placenta could be a protective response against oxidative stress, which may
772 explain why HMOX1 was higher in FGR placentae.
773
774 Our findings suggest a delicate balance in placental heme metabolism in FGR, whereby the
775 upregulation of heme synthesis pathways likely represents an adaptive response to
776 fetoplacental hypoxia and maintenance of placental bioenergetics. Simultaneously, the increase
777 in HMOX1-mediated heme catabolism serves as a protective mechanism against heme-induced
778 oxidative stress.
779
780 *Haematopoietic function in FGR placentae*
781 In addition to its role in mitochondrial function, heme is integral for the production of various
782 globin chains, including gamma (γ), alpha (α) and beta (β) (Figure 4). As we observed an
783 increase in heme-producing proteins, but no corresponding change in available heme in our
784 FGR placental tissue, we examined the intricate relationship between heme and globin
785 synthesis. This fundamental process is central to the oxygen-carrying capacity of blood and,
786 by extension, aerobic respiration essential for cellular function and viability (Hamza & Dailey,
787 2012; Voltarelli et al., 2023). During embryonic development, primitive embryonic
788 erythrocytes are located in blood islands of the secondary yolk sac (Manning *et al.*, 2020).
789 Subsequently, a crucial transition occurs, coinciding with placental formation and the

790 emergence of definitive erythropoiesis (Palis & Segel, 1998). This developmental shift results
791 in the production of fetal haemoglobin (α2γ2), which becomes the predominant form
792 throughout the remainder of fetal development (Hardison, 2012). This haemoglobin switching
793 process represents a critical milestone in fetal haematological development and is tightly
794 regulated by complex genetic and epigenetic factors (Hardison, 2012; Manning *et al.*, 2020).
795 Fetal haemoglobin production begins at around 10 weeks of gestation, peaking at 20 weeks and
796 remaining constant until the final month of fetal development when gamma-globin synthesis
797 rapidly decreases (Cantú & Philipsen, 2014; Mavilio *et al.*, 1983). Our findings revealed lower
798 protein abundance of gamma-1 (HBG1; 1.25-fold; 0.325 $\log_2$-FC) and gamma-2 (HBG2: 1.09-
799 fold; 0.09 $\log_2$-FC), key beta-like globin components of fetal haemoglobin, along with
800 haemoglobin subunit alpha 1 (HBA1; 1.16-fold; 0.21 $\log_2$-FC), in FGR placental tissue
801 compared to healthy term placental tissue (Figure 4). Additionally, the mRNA expression of
802 haemoglobin subunit beta (HBB; $p<0.05$), a critical component of adult haemoglobin ($\alpha_2\beta_2$),
803 was significantly increased in FGR placentae, however, protein abundance for HBB was 1.50-
804 fold lower (Figure 4D and G). The presence of HBB in the placenta aligns with current
805 literature stating that β-globin synthesis begins during the last month of fetal development
806 (Cantú & Philipsen, 2014). The switch from fetal to adult haemoglobin occurs when
807 erythropoiesis shifts from the fetal liver to the bone marrow at approximately (Khandros &
808 Blobel, 2024).
809
810 While fetal hypoxia in FGR is typically associated with elevated erythropoietin (EPO)
811 production and increased fetal haemoglobin synthesis (Chang *et al.*, 2018), our findings
812 indicate a disruption in globin chain production. The lower protein abundance of key globin
813 subunits, HBG1, HBG2, HBB and HBA1, in FGR placental tissue, suggests that globin chain
814 synthesis or stability may be impaired, potentially limiting the assembly of functional
815 haemoglobin. Although recent studies describe the placenta as a transient hematopoietic niche,
816 particularly during early to mid-gestation (Ivanovs *et al.*, 2017; Rhodes *et al.*, 2008), this
817 function may be compromised in FGR. Chronic hypoxia, inflammation, and oxidative stress,
818 all hallmarks of FGR pathophysiology, can disrupt haematopoietic stem and progenitor cell
819 (HSPC) function and erythroid differentiation (Dzierzak & Bigas, 2018). While hypoxia is
820 known to drive the upregulation of fetal haemoglobin via HIF1α activation (Khandros &
821 Blobel, 2024), we instead observed lower levels of subunits in both fetal and adult
822 haemoglobin. Together, suggesting a dysfunctional placental erythropoietic environment in
823 FGR.
824

825 Given the substantial alterations in both heme and globin subunits, we further investigated the
826 erythropoietic structure in the FGR placenta. Our study revealed significant alterations in key
827 structural proteins within FGR placentae. Notably, we observed reductions in erythrocyte
828 membrane protein band 4.1 (EPB41) expression at both mRNA ($p<0.05$) and protein levels
829 (1.19-fold; 0.253 $\log_2$-FC) in FGR placentae (Figure 4E and G). The crucial role of EPB41 is
830 in stabilising the actin-spectrin cytoskeleton of erythrocytes, thereby maintaining the
831 characteristic biconcave disc shape of erythrocytes. The biconcave shape is fundamental to
832 erythrocytes' function, optimising surface area to volume ratio and facilitating efficient oxygen
833 diffusion and laminar flow in circulation (Uzoigwe, 2006; Vorn *et al.*, 2023). Huang et al (2017)
834 showed that EPB41 null mice failed to develop a biconcave shape, resulting in compromised
835 oxygen diffusion capacity. Furthermore, we observed reduced protein abundance in EPB42
836 (1.48-fold; 0.562 $\log_2$-FC), SPTA1 (1.12-fold; 0.153 $\log_2$-FC), SPTB (1.40-fold; 0.0491 $\log_2$-
837 FC), ANK1 (1.57-fold; 0.661 $\log_2$-FC) and SLC4A1 (1.40-fold; 0.493 $\log_2$-FC) in FGR
838 placentae when compared to healthy controls (Figure 4G). Similarly, these proteins are integral
839 components of the erythrocyte membrane, conferring flexibility and stability (Alper, 2009; Guo
840 *et al.*, 2022; Vorn *et al.*, 2023) Mutations in the aforementioned genes have been implicated in
841 hereditary spherocytosis (Xu *et al.*, 2023), a condition characterised by erythrocyte membrane
842 instability and deformation. Our findings suggest altered erythropoietic structure during
843 erythrocyte maturation, as HEMGN mRNA expression remained unchanged, indicating that
844 the HSPC population and early erythroid commitment remain preserved.
845
846 We propose that changes in the erythropoietic structure reflects a hypoxia-driven alteration in
847 erythroid maturation, skewing erythropoiesis toward a rapid, stress-induced phenotype
848 regulated in part by HIFs (Haase, 2013). Hypoxia-induced oxidative stress, as characteristic of
849 FGR (Xu *et al.*, 2021), has been shown to affect the post-translational folding or stability of
850 erythrocyte membrane components, which may further affect the abundance of EPB41 and
851 EPB42 (Mohandas & Gallagher, 2008) and other erythrocyte membrane-bound proteins.
852 Stress-induced erythropoiesis favours accelerated erythropoiesis, which may compromise
853 erythrocyte cytoskeletal assembly and membrane protein integration (Paulson *et al.*, 2020).
854 Collectively, these alterations may represent an attempt to increase erythrocyte deformability
855 to facilitate circulation within the structurally compromised vasculature of the FGR placenta,
856 characterised by narrower blood vessels and increased vascular resistance (Boss *et al.*, 2023;
857 Kovo *et al.*, 2013; Sun *et al.*, 2020). Thus, enabling efficient uptake and transport of the limited
858 oxygen available to the fetus.
859

Despite the structural and functional changes observed in erythrocytes of FGR placental tissue, the mRNA expression of hemogen (HEMGN) remained unchanged. Hemogen regulates the proliferation and differentiation of haematopoietic cells (Jiang *et al.*, 2023) indicating that the architectural insult observed in FGR placentae is likely not occurring during haematopoiesis but rather during erythrocyte maturation (Vorn *et al.*, 2023) or as a result of stress-induced erythrocyte maturation (Paulson *et al.*, 2020).

Limitations

While previous research indicates that maternal iron status is a critical determinant of fetal iron acquisition through placental transport (Cao & Fleming, 2016; Fisher & Nemeth, 2017; Roberts *et al.*, 2020), our study has provided new insights into intrinsic placental changes that are independent of maternal iron status, revealing potential intracellular alterations that have remained elusive in the development of FGR. Since, the placenta is the critical interface between maternal and fetal circulations, building upon the biomolecular foundation established in this study incorporating fetal cord blood analysis in future studies would provide further insight into how modifications in placental iron transport and utilisation impact fetal iron status. In this study, maternal patient records were retrieved from mothers who delivered either healthy or FGR infants, offering valuable insights into maternal iron status during pregnancy. The clinical records revealed comparable iron parameters between groups, strengthening our conclusion that the placental iron alterations we observed represent intrinsic placental adaptations rather than responses to maternal iron availability. Although the retrospective nature of clinical records means that iron parameters were measured based on clinical need rather than a standardised gestational timepoint. While this approach provides real-time data collected during routine clinical care, data uniformity across participants may be potentially limiting (Talari & Goyal, 2020).

This study employed a bottom-up liquid chromatography mass spectrometry (LC-MS) proteomic approach to successfully identify significant alterations in placental iron transport and mitochondrial iron utilisation. While the LC-MS methodology chosen is well-suited to global profiling performed within this study to assess total cellular protein content, some proteins were difficult to detect due to protein inference ambiguity, underrepresentation of low-abundance, membrane-bound proteins, and incomplete coverage of post-translational modifications (Bruderer *et al.*, 2015; Mulhall *et al.*). Notably, key Fe-S cluster proteins essential for de novo and late-stage synthesis were difficult to detect, likely due to their hydrophobic nature and the inherent limitations of the protocol (Mulhall *et al.*). Future studies

incorporating targeted approaches may improve the detection and quantification of such proteins.

Our study primarily focused on non-heme iron pathways within the placenta, which represents 85% of iron obtained from the maternal diet through plant-based sources of iron (Piskin *et al.*, 2022; Yiannikourides & Latunde-Dada, 2019). Heme-iron, accounting for 15% of dietary iron from animal-based sources, requires further investigation to understand heme-iron absorption during pregnancy. Current literature suggests that heme-iron absorption follows the same pattern as non-heme iron absorption in the placenta and is mainly sourced via maternal haemolysis rather than absorbed dietary iron (Milman, 2006; Roberts *et al.*, 2020).

Conclusion

Our study reveals specific alterations in placental iron transport and utilisation pathways in FGR, that are independent of maternal iron status. We identified increased placental iron transporters alongside reduced ferroportin, suggesting an adaptive iron retention within FGR placentae. Assessment of mitochondrial iron utilisation pathways in FGR placentae suggested a preference for [2Fe-2S] cluster formation and heme synthesis over [4Fe-4S] cluster assembly in FGR. Collectively, these findings of altered placental iron transporters and modifications in mitochondrial Fe-S cluster and heme synthesis pathways likely reflect the placenta's response to the compromised vascular environment characteristic of FGR. We also observed reduced haemoglobin subunits and changes in erythrocyte structural proteins in FGR placentae, indicative of altered placental hematopoietic function. We propose these data are a programmed response to hypoxia and stress-induced haematopoiesis to overcome the poor placental vasculature in FGR. Together, these findings provide new insights into how alterations in iron transport and iron-dependent pathways contribute to the development of FGR.

Data Availability Statement

The authors will make the raw data supporting the conclusions of this article available, without undue reservation, to any qualified researcher.

Funding

This research was supported by the National Health and Medical Research Council Investigator Grant GNT2026065.

Author Contributions

VBB, KGP, RS and JJF contributed to the conception and design of the study. VBB, HM and SA contributed to the acquisition, analysis and interpretation of data for the study. VBB, KGP, RS, and JJF contributed to drafting the work and critically revising the intellectual content. All authors have approved the final version of the manuscript. All authors agree to be accountable for all aspects of the work. All persons designated as authors qualify for authorship and are listed.

Competing Interests

The authors declare that they have no conflict of interest in this study.

Acknowledgements

We gratefully acknowledge the research midwives at John Hunter Hospital, Skye Doel and Bridget McCleery, who were involved in participant recruitment and clinical data collection, for their invaluable support and contribution to this study.

References

Abbassi-Ghanavati M, Greer LG & Cunningham FG. (2009). Pregnancy and laboratory studies: a reference table for clinicians. *Obstet Gynecol* **114,** 1326-1331.

Al-Karadaghi S, Hansson M, Nikonov S, Jönsson B & Hederstedt L. (1997). Crystal structure of ferrochelatase: the terminal enzyme in heme biosynthesis. *Structure* **5,** 1501-1510.

Ali MY, Oliva CR, Flor S & Griguer CE. (2022). Mitoferrin, Cellular and Mitochondrial Iron Homeostasis. *Cells* **11**.

Allerkamp HH, Pole T, Boukham A, James JL & Clark AR. (2022). Pregnancy-specific uterine vascular reactivity: a data-driven computational model of shear-dependent, myogenic, and mechanical radial artery features. *American Journal of Physiology-Heart and Circulatory Physiology* **323,** H72-H88.

Alper SL. (2009). Molecular physiology and genetics of Na+-independent SLC4 anion exchangers. *J Exp Biol* **212,** 1672-1683.

Amick J, Schlanger SE, Wachnowsky C, Moseng MA, Emerson CC, Dare M, Luo WI, Ithychanda SS, Nix JC, Cowan JA, Page RC & Misra S. (2014). Crystal structure of the nucleotide-binding domain of mortalin, the mitochondrial Hsp70 chaperone. *Protein Sci* **23,** 833-842.

Anderson GJ & Frazer DM. (2017). Current understanding of iron homeostasis. *Am J Clin Nutr* **106,** 1559s-1566s.

Andrews NC. (2000). Iron metabolism: iron deficiency and iron overload. *Annu Rev Genomics Hum Genet* **1,** 75-98.

Aye I, Aiken CE, Charnock-Jones DS & Smith GCS. (2022). Placental energy metabolism in health and disease-significance of development and implications for preeclampsia. *Am J Obstet Gynecol* **226,** S928-s944.

Beilschmidt LK, Ollagnier de Choudens S, Fournier M, Sanakis I, Hograindleur MA, Clémancey M, Blondin G, Schmucker S, Eisenmann A, Weiss A, Koebel P, Messaddeq N, Puccio H & Martelli A. (2017). ISCA1 is essential for mitochondrial Fe(4)S(4) biogenesis in vivo. *Nat Commun* **8,** 15124.

Boss AL, Chamley LW, Brooks AES & James JL. (2023). Human placental vascular and perivascular cell heterogeneity differs between first trimester and term, and in pregnancies affected by foetal growth restriction. *Mol Hum Reprod* **29**.

Brighton E. (2019). New South Wales Hopsital Laboratory clinical projects laboratory manaual ed. 2019 NRRA. NSW Health Pathology.

Brooker I, Fisher J, Delforce S, Endacott S, Lumbers E, Sutherland J & Pringle K. (2025). Characterising the role of placental angiotensin-converting enzyme 2 (ACE2) during the onset of oxidative insult by hypoxia/reoxygenation: Implications for fetal growth restriction. *Placenta* **165**.

Bruderer R, Bernhardt OM, Gandhi T, Miladinović SM, Cheng L-Y, Messner S, Ehrenberger T, Zanotelli V, Butscheid Y, Escher C, Vitek O, Rinner O & Reiter L. (2015). Extending the Limits of Quantitative Proteome Profiling with Data-Independent Acquisition and Application to Acetaminophen-Treated Three-Dimensional Liver Microtissues*[S]. *Molecular & Cellular Proteomics* **14,** 1400-1410.

Burton G & Fowden A. (2012). The placenta and developmental programming: balancing fetal nutrient demands with maternal resource allocation. *Placenta* **33,** S23-S27.

Burton GJ & Jauniaux E. (2018). Pathophysiology of placental-derived fetal growth restriction. *Am J Obstet Gynecol* **218,** S745-s761.

Camaschella C. (2015). Iron-deficiency anemia. *N Engl J Med* **372,** 1832-1843.

Cantú I & Philipsen S. (2014). Flicking the switch: Adult hemoglobin expression in erythroid cells derived from cord blood and human induced pluripotent stem cells. *Haematologica* **99,** 1647-1649.

Cao C & Fleming MD. (2016). The placenta: the forgotten essential organ of iron transport. *Nutr Rev* **74,** 421-431.

Cerami C. (2017). Iron Nutriture of the Fetus, Neonate, Infant, and Child. *Ann Nutr Metab* **71 Suppl 3,** 8-14.

Chang Y-L, Chao A-S, Peng H-H, Chang S-D, Chen K-J, Cheng P-J & Wang T-H. (2018). Placental erythropoietin expression is upregulated in growth-restricted fetuses with abnormal umbilical artery Doppler findings: a case–control study of monochorionic twins. *BMC Pregnancy and Childbirth* **18,** 1-7.

Chiabrando D, Mercurio S & Tolosano E. (2014). Heme and erythropoieis: more than a structural role. *Haematologica* **99,** 973-983.

Cindrova-Davies T & Sferruzzi-Perri AN. (2022). Human placental development and function. *Semin Cell Dev Biol* **131,** 66-77.

de Freitas MAR, da Costa AV, Medeiros LA, Cunha LM, Coutinho Filho U, Garrote Filho MdS, Diniz ALD & Penha-Silva N. (2019). The role of the erythrocyte in the outcome of pregnancy with preeclampsia. *PLOS ONE* **14,** e0212763.

Delaney KM, Guillet R, Pressman EK, Ganz T, Nemeth E & O'Brien KO. (2021). Serum Erythroferrone During Pregnancy Is Related to Erythropoietin but Does Not Predict the Risk of Anemia. *The Journal of Nutrition* **151,** 1824-1833.

Dev S & Babitt JL. (2017). Overview of iron metabolism in health and disease. *Hemodial Int* **21 Suppl 1,** S6-s20.

Dores-Silva PR, Barbosa LR, Ramos CH & Borges JC. (2015). Human mitochondrial Hsp70 (mortalin): shedding light on ATPase activity, interaction with adenosine nucleotides, solution structure and domain organization. *PLoS One* **10,** e0117170.

Dzierzak E & Bigas A. (2018). Blood development: hematopoietic stem cell dependence and independence. *Cell stem cell* **22,** 639-651.

Fairchild Benyo D & Conrad KP. (1999). Expression of the erythropoietin receptor by trophoblast cells in the human placenta. *Biology of reproduction* **60,** 861-870.

Fava C, Cattazzo F, Hu ZD, Lippi G & Montagnana M. (2019). The role of red blood cell distribution width (RDW) in cardiovascular risk assessment: useful or hype? *Ann Transl Med* **7,** 581.

Fisher AL & Nemeth E. (2017). Iron homeostasis during pregnancy. *Am J Clin Nutr* **106,** 1567s-1574s.

Fisher JJ, Grace T, Castles NA, Jones EA, Delforce SJ, Peters AE, Crombie GK, Hoedt EC, Warren KE, Kahl RG, Hirst JJ, Pringle KG & Pennell CE. (2024). Methodology for Biological Sample Collection, Processing, and Storage in the Newcastle 1000 Pregnancy Cohort: Protocol for a Longitudinal, Prospective Population-Based Study in Australia. *JMIR Res Protoc* **13,** e63562.

Fisher JJ, McKeating DR, Cuffe JS, Bianco-Miotto T, Holland OJ & Perkins AV. (2019). Proteomic analysis of placental mitochondria following trophoblast differentiation. *Frontiers in physiology* **10,** 1536.

Gambling L, Danzeisen R, Gair S, Lea RG, Charania Z, Solanky N, Joory KD, Srai SK & McArdle HJ. (2001). Effect of iron deficiency on placental transfer of iron and expression of iron transport proteins in vivo and in vitro. *Biochem J* **356,** 883-889.

Gekas C, Dieterlen-Lièvre F, Orkin SH & Mikkola HK. (2005). The placenta is a niche for hematopoietic stem cells. *Dev Cell* **8,** 365-375.

Gekas C, Rhodes KE, Van Handel B, Chhabra A, Ueno M & Mikkola HK. (2010). Hematopoietic stem cell development in the placenta. *Int J Dev Biol* **54,** 1089-1098.

Gordijn SJ, Beune IM, Thilaganathan B, Papageorghiou A, Baschat AA, Baker PN, Silver RM, Wynia K & Ganzevoort W. (2016). Consensus definition of fetal growth restriction: a Delphi procedure. *Ultrasound in Obstetrics & Gynecology* **48,** 333-339.

Guan S, Zhao L & Peng R. (2022). Mitochondrial Respiratory Chain Supercomplexes: From Structure to Function. *Int J Mol Sci* **23**.

Guo S, Frazer DM & Anderson GJ. (2016). Iron homeostasis: transport, metabolism, and regulation. *Curr Opin Clin Nutr Metab Care* **19,** 276-281.

Guo X, Zhao Y, Kim J & Dean A. (2022). Hemogen/BRG1 cooperativity modulates promoter and enhancer activation during erythropoiesis. *Blood* **139,** 3532-3545.

Guo Y, Zhang N, Zhang D, Ren Q, Ganz T, Liu S & Nemeth E. (2019). Iron homeostasis in pregnancy and spontaneous abortion. *American journal of hematology* **94,** 184-188.

Haase VH. (2013). Regulation of erythropoiesis by hypoxia-inducible factors. *Blood Reviews* **27,** 41-53.

Hardison RC. (2012). Evolution of hemoglobin and its genes. *Cold Spring Harbor perspectives in medicine* **2,** a011627.

Hentze MW, Muckenthaler MU & Andrews NC. (2004). Balancing Acts: Molecular Control of Mammalian Iron Metabolism. *Cell* **117,** 285-297.

Herrera MG, Noguera ME, Sewell KE, Agudelo Suárez WA, Capece L, Klinke S & Santos J. (2019). Structure of the Human ACP-ISD11 Heterodimer. *Biochemistry* **58,** 4596-4609.

Higashijima A, Miura K, Mishima H, Kinoshita A, Jo O, Abe S, Hasegawa Y, Miura S, Yamasaki K, Yoshida A, Yoshiura K-i & Masuzaki H. (2013). Characterization of placenta-specific microRNAs in fetal growth restriction pregnancy. *Prenatal Diagnosis* **33,** 214-222.

Holland O, Dekker Nitert M, Gallo LA, Vejzovic M, Fisher JJ & Perkins AV. (2017). Review: Placental mitochondrial function and structure in gestational disorders. *Placenta* **54,** 2-9.

Hou J, Cliver SP, Tamura T, Johnston KE & Goldenberg R. (2000). Maternal serum ferritin and fetal growth. *Obstet Gynecol* **95,** 447-452.

Ivanovs A, Rybtsov S, Ng ES, Stanley EG, Elefanty AG & Medvinsky A. (2017). Human haematopoietic stem cell development: from the embryo to the dish. *Development* **144,** 2323-2337.

Jiang Y, Yu L, Hu Q, Kang Y, You J, Huang C, Xu X & Chen L. (2023). Cancer/testis antigen HEMGN correlated with immune infiltration serves as a prognostic biomarker in lung adenocarcinoma. *Mol Immunol* **153,** 226-237.

Kautz L & Nemeth E. (2014). Molecular liaisons between erythropoiesis and iron metabolism. *Blood* **124,** 479-482.

Khandros E & Blobel GA. (2024). Elevating fetal hemoglobin–recently discovered regulators and mechanisms. *Blood*.

Kim HJ, Khalimonchuk O, Smith PM & Winge DR. (2012). Structure, function, and assembly of heme centers in mitochondrial respiratory complexes. *Biochimica et Biophysica Acta (BBA)-Molecular Cell Research* **1823,** 1604-1616.

Kovo M, Schreiber L, Ben-Haroush A, Cohen G, Weiner E, Golan A & Bar J. (2013). The placental factor in early- and late-onset normotensive fetal growth restriction. *Placenta* **34,** 320-324.

Kurt RK, Aras Z, Silfeler DB, Kunt C, Islimye M & Kosar O. (2015). Relationship of Red Cell Distribution Width With the Presence and Severity of Preeclampsia. *Clinical and Applied Thrombosis/Hemostasis* **21,** 128-131.

Lee D-C, Romero R, Kim J-S, Tarca AL, Montenegro D, Pineles BL, Kim E, Lee J, Kim SY, Draghici S, Mittal P, Kusanovic JP, Chaiworapongsa T, Hassan SS & Kim CJ. (2011). miR-210 Targets Iron-Sulfur Cluster Scaffold Homologue in Human Trophoblast Cell Lines: Siderosis of Interstitial Trophoblasts as a Novel Pathology of Preterm Preeclampsia and Small-for-Gestational-Age Pregnancies. *The American Journal of Pathology* **179,** 590-602.

Lippi G & Plebani M. (2014). Red blood cell distribution width (RDW) and human pathology. One size fits all. *Clinical Chemistry and Laboratory Medicine (CCLM)* **52,** 1247-1249.

Maio N & Rouault TA. (2020). Outlining the Complex Pathway of Mammalian Fe-S Cluster Biogenesis. *Trends Biochem Sci* **45,** 411-426.

Maio N & Rouault TA. (2020). Outlining the Complex Pathway of Mammalian Fe-S Cluster Biogenesis. *Trends in Biochemical Sciences* **45,** 411-426.

Manning JM, Manning LR, Dumoulin A, Padovan JC & Chait B. (2020). Embryonic and Fetal Human Hemoglobins: Structures, Oxygen Binding, and Physiological Roles. In *Vertebrate and Invertebrate Respiratory Proteins, Lipoproteins and other Body*

Fluid Proteins, ed. Hoeger U & Harris JR, pp. 275-296. Springer International Publishing, Cham.

Mastrogiannaki M, Matak P, Keith B, Simon MC, Vaulont S & Peyssonnaux C. (2009). HIF-2alpha, but not HIF-1alpha, promotes iron absorption in mice. *J Clin Invest* **119,** 1159-1166.

Mavilio F, Giampaolo A, Carè A, Migliaccio G, Calandrini M, Russo G, Pagliardi GL, Mastroberardino G, Marinucci M & Peschle C. (1983). Molecular mechanisms of human hemoglobin switching: selective undermethylation and expression of globin genes in embryonic, fetal, and adult erythroblasts. *Proc Natl Acad Sci U S A* **80,** 6907-6911.

McArdle HJ, Danzeisen R, Fosset C & Gambling L. (2003). The role of the placenta in iron transfer from mother to fetus and the relationship between iron status and fetal outcome. *Biometals* **16,** 161-167.

McArdle HJ, Lang C, Hayes H & Gambling L. (2011). Role of the placenta in regulation of fetal iron status. *Nutr Rev* **69 Suppl 1,** S17-22.

Mecacci F, Avagliano L, Lisi F, Clemenza S, Serena C, Vannuccini S, Rambaldi MP, Simeone S, Ottanelli S & Petraglia F. (2021). Fetal Growth Restriction: Does an Integrated Maternal Hemodynamic-Placental Model Fit Better? *Reprod Sci* **28,** 2422-2435.

Mégier C, Peoc'h K, Puy V & Cordier AG. (2022). Iron Metabolism in Normal and Pathological Pregnancies and Fetal Consequences. *Metabolites* **12**.

Melber A, Na U, Vashisht A, Weiler BD, Lill R, Wohlschlegel JA & Winge DR. (2016). Role of Nfu1 and Bol3 in iron-sulfur cluster transfer to mitochondrial clients. *Elife* **5,** e15991.

Miller J, Turan S & Baschat AA. (2008). Fetal Growth Restriction. *Seminars in Perinatology* **32,** 274-280.

Milman N. (2006). Iron and pregnancy--a delicate balance. *Ann Hematol* **85,** 559-565.

Mohandas N & Gallagher PG. (2008). Red cell membrane: past, present, and future. *Blood* **112,** 3939-3948.

Moksnes MR, Graham SE, Wu K-H, Hansen AF, Gagliano Taliun SA, Zhou W, Thorstensen K, Fritsche LG, Gill D, Mason A, Cucca F, Schlessinger D, Abecasis GR, Burgess S, Åsvold BO, Nielsen JB, Hveem K, Willer CJ & Brumpton BM. (2022). Genome-wide meta-analysis of iron status biomarkers and the effect of iron on all-cause mortality in HUNT. *Communications Biology* **5,** 591.

Mostajabi Sarhangi S & Matyushov DV. (2023). Electron Tunneling in Biology: When Does it Matter? *ACS Omega* **8,** 27355-27365.

Mulhall JE, Trigg NA, Bernstein IR, Anderson AL, Murray HC, Sipilä P, Lord T, Schjenken JE, Nixon B & Skerrett-Byrne DA. (2024). Immortalized mouse caput epididymal epithelial (mECap18) cell line recapitulates the in-vivo environment. *PROTEOMICS* **24,** 2300253.

Murray HC, Miller K, Brzozowski JS, Kahl RGS, Smith ND, Humphrey SJ, Dun MD & Verrills NM. (2023). Synergistic Targeting of DNA-PK and KIT Signaling Pathways in KIT Mutant Acute Myeloid Leukemia. *Molecular & Cellular Proteomics* **22,** 100503.

Nader E, Skinner S, Romana M, Fort R, Lemonne N, Guillot N, Gauthier A, Antoine-Jonville S, Renoux C, Hardy-Dessources M-D, Stauffer E, Joly P, Bertrand Y & Connes P. (2019). Blood Rheology: Key Parameters, Impact on Blood Flow, Role in Sickle Cell Disease and Effects of Exercise. *Frontiers in Physiology* **Volume 10 - 2019**.

Nasta V, Da Vela S, Gourdoupis S, Ciofi-Baffoni S, Svergun DI & Banci L. (2019). Structural properties of [2Fe-2S] ISCA2-IBA57: a complex of the mitochondrial iron-sulfur cluster assembly machinery. *Scientific Reports* **9,** 18986.

O'Brien KO. (2022). Maternal, fetal and placental regulation of placental iron trafficking. *Placenta* **125,** 47-53.

Obi CD, Bhuiyan T, Dailey HA & Medlock AE. (2022). Ferrochelatase: Mapping the Intersection of Iron and Porphyrin Metabolism in the Mitochondria. *Frontiers in Cell and Developmental Biology* **Volume 10 - 2022**.

Ozgu-Erdinc AS, Cavkaytar S, Aktulay A, Buyukkagnici U, Erkaya S & Danisman N. (2014). Mid-trimester maternal serum and amniotic fluid biomarkers for the prediction of preterm delivery and intrauterine growth retardation. *J Obstet Gynaecol Res* **40,** 1540-1546.

Palis J & Segel GB. (1998). Developmental biology of erythropoiesis. *Blood Reviews* **12,** 106-114.

Paradkar PN, Zumbrennen KB, Paw BH, Ward DM & Kaplan J. (2009). Regulation of mitochondrial iron import through differential turnover of mitoferrin 1 and mitoferrin 2. *Molecular and cellular biology* **29,** 1007-1016.

Paul BT, Manz DH, Torti FM & Torti SV. (2017). Mitochondria and Iron: current questions. *Expert Rev Hematol* **10,** 65-79.

Paulson RF, Hariharan S & Little JA. (2020). Stress erythropoiesis: definitions and models for its study. *Experimental hematology* **89,** 43-54. e42.

Perry H, Lehmann H, Mantovani E, Thilaganathan B & Khalil A. (2020). Are maternal hemodynamic indices markers of fetal growth restriction in pregnancies with a small-for-gestational-age fetus? *Ultrasound in Obstetrics & Gynecology* **55,** 210-216.

Piskin E, Cianciosi D, Gulec S, Tomas M & Capanoglu E. (2022). Iron Absorption: Factors, Limitations, and Improvement Methods. *ACS Omega* **7,** 20441-20456.

Qi Y, Hu M, Wang Z & Shang W. (2023). Mitochondrial iron regulation as an emerging target in ischemia/reperfusion injury during kidney transplantation. *Biochemical Pharmacology* **215,** 115725.

Read AD, Bentley RE, Archer SL & Dunham-Snary KJ. (2021). Mitochondrial iron-sulfur clusters: Structure, function, and an emerging role in vascular biology. *Redox Biol* **47,** 102164.

Reddy SG, Kumar H, Nagaraj G & Kottur PP. (2016). Red cell distribution width as a marker of preeclampsia severity. *Journal of Evolution of Medical and Dental Sciences* **5,** 3104-3108.

Rhodes KE, Gekas C, Wang Y, Lux CT, Francis CS, Chan DN, Conway S, Orkin SH, Yoder MC & Mikkola HK. (2008). The emergence of hematopoietic stem cells is initiated in the placental vasculature in the absence of circulation. *Cell stem cell* **2,** 252-263.

Roberts H, Bourque SL & Renaud SJ. (2020). Maternal iron homeostasis: effect on placental development and function. *Reproduction* **160,** R65-r78.

Robin C, Bollerot K, Mendes S, Haak E, Crisan M, Cerisoli F, Lauw I, Kaimakis P, Jorna R, Vermeulen M, Kayser M, van der Linden R, Imanirad P, Verstegen M, Nawaz-Yousaf H, Papazian N, Steegers E, Cupedo T & Dzierzak E. (2009). Human placenta is a potent hematopoietic niche containing hematopoietic stem and progenitor cells throughout development. *Cell Stem Cell* **5,** 385-395.

Sanghavi M & Rutherford JD. (2014). Cardiovascular Physiology of Pregnancy. *Circulation* **130,** 1003-1008.

Sangkhae V, Fisher AL, Wong S, Koenig MD, Tussing-Humphreys L, Chu A, Lelić M, Ganz T & Nemeth E. (2020). Effects of maternal iron status on placental and fetal iron homeostasis. *J Clin Invest* **130,** 625-640.

Semenza GL. (2014). Oxygen sensing, hypoxia-inducible factors, and disease pathophysiology. *Annu Rev Pathol* **9,** 47-71.

Shaw GC, Cope JJ, Li L, Corson K, Hersey C, Ackermann GE, Gwynn B, Lambert AJ, Wingert RA, Traver D, Trede NS, Barut BA, Zhou Y, Minet E, Donovan A, Brownlie A, Balzan R, Weiss MJ, Peters LL, Kaplan J, Zon LI & Paw BH. (2006). Mitoferrin is essential for erythroid iron assimilation. *Nature* **440,** 96-100.

Shehata HA, Ali MM, Evans-Jones JC, Upton GJG & Manyonda IT. (1998). Red cell distribution width (RDW) changes in pregnancy. *International Journal of Gynecology & Obstetrics* **62,** 43-46.

Shi Y, Ghosh M, Kovtunovych G, Crooks DR & Rouault TA. (2012). Both human ferredoxins 1 and 2 and ferredoxin reductase are important for iron-sulfur cluster biogenesis. *Biochimica et Biophysica Acta (BBA) - Molecular Cell Research* **1823,** 484-492.

Sibley CP, Brownbill P, Dilworth M & Glazier JD. (2010). Adaptation in placental nutrient supply to meet fetal growth demand: implications for programming. *Placenta* **31,** S70-S74.

Söhnchen N, Melzer K, Tejada BMd, Jastrow-Meyer N, Othenin-Girard V, Irion O, Boulvain M & Kayser B. (2011). Maternal heart rate changes during labour. *European Journal of Obstetrics & Gynecology and Reproductive Biology* **158,** 173-178.

Sun C, Groom KM, Oyston C, Chamley LW, Clark AR & James JL. (2020). The placenta in fetal growth restriction: What is going wrong? *Placenta* **96,** 10-18.

Talari K & Goyal M. (2020). Retrospective studies - utility and caveats. *J R Coll Physicians Edinb* **50,** 398-402.

Tang L, He G, Liu X & Xu W. (2017). Progress in the understanding of the etiology and predictability of fetal growth restriction. *Reproduction* **153,** R227-R240.

Uzoigwe C. (2006). The human erythrocyte has developed the biconcave disc shape to optimise the flow properties of the blood in the large vessels. *Med Hypotheses* **67,** 1159-1163.

Vanlander AV & Van Coster R. (2018). Clinical and genetic aspects of defects in the mitochondrial iron–sulfur cluster synthesis pathway. *JBIC Journal of Biological Inorganic Chemistry* **23,** 495-506.

Voltarelli VA, Alves de Souza RW, Miyauchi K, Hauser CJ & Otterbein LE. (2023). Heme: The Lord of the Iron Ring. *Antioxidants* **12,** 1074.

Vorn R, Devoto C, Meier TB, Lai C, Yun S, Broglio SP, Mithani S, McAllister TW, Giza CC, Kim H-S, Huber D, Harezlak J, Cameron KL, McGinty G, Jackson J, Guskiewicz KM, Mihalik JP, Brooks A, Duma S, Rowson S, Nelson LD, Pasquina P, McCrea MA & Gill JM. (2023). Are EPB41 and alpha-synuclein diagnostic biomarkers of sport-related concussion? Findings from the NCAA and Department of Defense CARE Consortium. *Journal of Sport and Health Science* **12,** 379-387.

Waldvogel-Abramowski S, Waeber G, Gassner C, Buser A, Frey BM, Favrat B & Tissot JD. (2014). Physiology of iron metabolism. *Transfus Med Hemother* **41,** 213-221.

Weiler BD, Brück M-C, Kothe I, Bill E, Lill R & Mühlenhoff U. (2020). Mitochondrial [4Fe-4S] protein assembly involves reductive [2Fe-2S] cluster fusion on ISCA1–ISCA2 by electron flow from ferredoxin FDX2. *Proceedings of the National Academy of Sciences* **117,** 20555-20565.

Wen Z, Luo D, Wang S, Rong R, Evers BM, Jia L, Fang Y, Daoud EV, Yang S, Gu Z, Arner EN, Lewis CM, Solis Soto LM, Fujimoto J, Behrens C, Wistuba, II, Yang DM, Brekken RA, O'Donnell KA, Xie Y & Xiao G. (2024). Deep Learning-Based H-Score Quantification of Immunohistochemistry-Stained Images. *Mod Pathol* **37,** 100398.

Wu BA, Chand KK, Bell A, Miller SL, Colditz PB, Malhotra A & Wixey JA. (2023). Effects of fetal growth restriction on the perinatal neurovascular unit and possible treatment targets. *Pediatric Research*.

Xu L, Wei X, Liang G, Zhu D, Zhang Y, Zhang Y & Shang X. (2023). A novel splicing mutation of ANK1 is associated with phenotypic heterogeneity of hereditary spherocytosis in a Chinese family. *Biochimica et Biophysica Acta (BBA) - Molecular Basis of Disease* **1869,** 166595.

Xu Y-Y, Liu Y, Cui L, Wu W-B, Quinn MJ, Menon R & Zhang H-J. (2021). Hypoxic effects on the mitochondrial content and functions of the placenta in fetal growth restriction. *Placenta* **114,** 100-107.

Yiannikourides A & Latunde-Dada GO. (2019). A Short Review of Iron Metabolism and Pathophysiology of Iron Disorders. *Medicines (Basel)* **6**.

Zaugg J, Lopez-Tello J, Musial B, Vaughan OR, Fowden AL, Albrecht C & Sferruzzi-Perri AN. (2024). Obesogenic diet in pregnancy disrupts placental iron handling and ferroptosis and stress signalling in association with fetal growth alterations. *Cellular and Molecular Life Sciences* **81,** 151.

Zaugg J, Solenthaler F & Albrecht C. (2022). Materno-fetal iron transfer and the emerging role of ferroptosis pathways. *Biochem Pharmacol* **202,** 115141.

Zhang J, Johnson PC & Popel AS. (2009). Effects of erythrocyte deformability and aggregation on the cell free layer and apparent viscosity of microscopic blood flows. *Microvasc Res* **77,** 265-272.

Zhong H, Janer A, Khalimonchuk O, Antonicka H, Shoubridge Eric A & Barrientos A. (2023). BOLA3 and NFU1 link mitoribosome iron–sulfur cluster assembly to multiple mitochondrial dysfunctions syndrome. *Nucleic Acids Research* **51,** 11797-11812.

Zygmunt M, Herr F, Münstedt K, Lang U & Liang OD. (2003). Angiogenesis and vasculogenesis in pregnancy. *European Journal of Obstetrics & Gynecology and Reproductive Biology* **110,** S10-S18.